Sucralose consumption ablates cancer immunotherapy response through microbiome disruption.

Kristin M Morder[1,2,#], Madison Nguyen[1,#], Drew N Wilfahrt[1,2,#], Zakaria Larbi Dahmani[2,3,], Ansen BP Burr[1,4], Bingxian Xie[1,2], Michael Morikone[5], Hector Nieves-Rosado[2,4], William G Gunn[1,2], Drew E Hurd[1], Hong Wang[1,6], Steven J Mullett[7], Kaitlin Bossong[1,2], Stacy L Gelhaus[7], Dhivyaa Rajasundaram[5], Lawrence P Kane[2], Greg M Delgoffe[1,2,8], Jishnu Das[2,3], Diwakar Davar[1,4,9]*, Abigail E Overacre-Delgoffe[1,2,8,10]*.

Running Title: Sucralose-driven microbiome changes limit immunotherapy

Affiliations:

[1]UPMC Hillman Cancer Center; Pittsburgh, 15213, USA.

[2]Department of Immunology, University of Pittsburgh; Pittsburgh, 15213, USA.

[3]Center for Systems Immunology; Pittsburgh, 15213, USA.

[4]Department of Medicine, University of Pittsburgh; Pittsburgh, 15213, USA.

[5]Bioinformatics Core, Department of Pediatrics, University of Pittsburgh; Pittsburgh, PA, 15213, USA.

[6]Biostatistics Facility, UPMC Hillman Cancer Center, University of Pittsburgh; Pittsburgh, 15213, USA.

[7]Department of Pharmacology and Chemical Biology, University of Pittsburgh; Pittsburgh, 15261, USA.

[8]Tumor Microenvironment Center; Pittsburgh, 15213, USA.

[#] contributed equally.

[9]Senior Author

[10]Lead Author

*Corresponding authors.

Abigail Overacre-Delgoffe; 5051 Centre Ave, 4047, Pittsburgh, PA 15213; overacre@pitt.edu; 412-648-4828

Diwakar Davar; 5117 Centre Ave, 1.32d, Pittsburgh, PA 15232; davard@upmc.edu; 412-692-4724

Competing interests:

DD: Data and Safety Monitoring Board (DSMB): Immunocore, Replimmune. Scientific Advisory Board (no stock): ACM Bio. Consultancy with compensation: ACM Bio, Ascendis, Castle, Clinical Care Options (CCO), Gerson Lehrman Group (GLG), Immunitas, Medical Learning Group (MLG), Replimmune, Trisalus, Xilio Therapeutics. Grants/Research Support (institutional): Arcus, Immunocore, Merck, Regeneron Pharmaceuticals Inc., Tesaro/GSK. CE Speakers' Bureau: Castle Biosciences, Regeneron. Stockholder: mBiomics, Zola. Intellectual Property: US Patent 63/124,231, "Compositions and Methods for Treating Cancer", Dec 11, 2020 US Patent 63/208,719, "Compositions and Methods For Responsiveness to Immune Checkpoint Inhibitors (ICI), Increasing Effectiveness of ICI and Treating Cancer", June 9, 2021

Abstract:

Gut microbiota composition is directly associated with response to immunotherapies in cancer. How the diet impacts the gut microbiota and downstream immune responses to cancer remains unclear. Here, we show that consumption of a common non-nutritive sweetener, sucralose, modifies microbiome composition, restricts T cell metabolism and function, and limits immunotherapy response in preclinical models of cancer and advanced cancer patients treated with anti-PD-1 based immune checkpoint inhibitors (ICIs). Sucralose consumption is associated with a reduction in microbiota-accessible arginine, and amino acid supplementation or fecal microbiome transfer (FMT) from anti-PD-1 responder mice completely restores T cell function and immunotherapy response. Overall, sucralose consumption destabilizes the gut microbiota, resulting in compromised T cell function and ablated ICI response in cancer.

Statement of Significance: This study highlights an unappreciated role of sucralose in reducing immunotherapy efficacy in both mouse models and cancer patient samples through shifts in the microbiome and arginine degradation that leads to T cell exhaustion. T cell function and immunotherapy responses are restored through amino acid supplementation.

Introduction

Immune checkpoint inhibitors (ICI) targeting negative regulatory checkpoints including programmed death-1 (PD-1) and cytotoxic T-lymphocyte-associated protein 4 (CTLA-4) produce durable responses in many cancers(1). In multiple cancers including melanoma and non-small cell lung cancer (NSCLC), ICIs singly or in combination with other agents including chemotherapy or tyrosine kinase inhibitors, produce high objective response rates (ORRs), and durable progression-free survival (PFS) and overall survival (OS) (2). However, the majority of ICI-treated patients fail to respond durably, and biomarkers are needed to tailor the management in these patients. Multiple predictive biomarkers of ICI response have been described including CD8+ TIL-infiltrate(3,4), PD-L1 expression(5,6), tumor mutation burden (TMB) (7,8), HLA class I haplotype(9). Recently, the gut microbiome has emerged as a major tumor-extrinsic regulator of response to multiple immunotherapies in human cancer patients including ICIs and anti-CD19 chimeric antigen receptor (CAR) T cell therapy(10–14). The gut microbiota can be shaped and altered by external factors including but not limited to host diet, antibiotic or probiotic use, and chemical exposures (15–19)[,](12).

Over the past several decades, humans have experienced major dietary changes, particularly a reduction in fiber intake in Westernized populations, which has parallelled general loss in the diversity of gut microbiota in Westernized populations compared to non-industrialized populations(20–22). These dietary changes have fueled a rise in obesity in industrialized countries(23). Non-nutritive sweeteners (NNS) were developed as an alternative to sugar, and NNS consumption has historically been considered safe and beneficial owing to their low caloric content, although the data underlying this is scarce. NNS intake is prevalent in the general population, both in lean and obese individuals alike, with 24-37% of United States adults reporting some NNS intake in dietary recall surveys(20). Two of the most used NNS, sucralose and saccharin, have been shown to significantly change the gut microbiome in mice and humans(24,25). Moreover, sucralose-induced microbial shifts are sufficient to negatively impact overall host health, including driving glucose intolerance(24–26). Further, while high doses of sucralose directly impairs T cell proliferation and effector function in preclinical models of autoimmune disease (27), the link between NNS intake in general, and sucralose

intake in particular, gut microbiota and immunotherapy outcomes in cancer is not well understood.

In this study, we observed that sucralose intake negatively impacted anti-PD-1 ICI efficacy in cancer in both mice and humans. In ICI-treated advanced melanoma, advanced NSCLC, and high-risk resectable melanoma patients, food frequency questionnaire (FFQ)-determined weight-normalized higher sucralose intake was associated with lower response and poorer survival compared to lower or no sucralose intake. Tumor-bearing mice given sucralose have poor responses to anti-PD-1 blockade, and this effect requires sucralose-driven changes to the gut microbiota. Overall, these findings suggest that high intake of sucralose contributes to ICI non-response in a gut microbiota-dependent T cell-centric fashion across preclinical models and cancer patients.

Results

Sucralose ablates immunotherapeutic response.

To evaluate whether sucralose intake impacted efficacy of anti-PD-1 ICI, we evaluated 3 separate cohorts of ICI-treated patients spanning a spectrum of histologies and stages: ICI-treated advanced melanoma, ICI-treated advanced NSCLC, and high-risk resectable melanoma treated with neoadjuvant ICI and TLR9 agonist vidutolimod (**Supplementary Fig. S1a**). Patients with advanced metastatic cutaneous melanoma or NSCLC who were scheduled to be treated with systemic anti-PD-1 based immunotherapy or chemoimmunotherapy were enrolled in a prospective research registry (HCC 20-019) that included administration of a validated web-based semiquantitative Diet History Questionnaire III (DHQ III) food frequency questionnaire (FFQ) that quantified self-reported dietary intake (**Supplementary Fig. S1a, Appendix 1-2**). Briefly, advanced melanoma or NSCLC patients who had received systemic anti-PD-1 based immunotherapy or chemoimmunotherapy, had undergone dietary history evaluation using DHQ III, had received treatment for at least 3 months, had at least 1 post-treatment imaging study evaluable for response, had adequate follow up time (6 months) and had provided informed consent were included (**Fig. 1a, Supplementary Fig. S1a**). Separately, we evaluated 25 patients with high-risk resectable melanoma

who received neoadjuvant anti-PD-1 nivolumab along with intratumoral TLR9 agonist vidutolimod, the primary results of which have previously been reported (**Supplementary Fig. S1a, Appendix 3-4**) (28). Overall, we included 91 advanced melanoma patients, 41 advanced NSCLC patients, and 25 high-risk resectable melanoma patients (**Supplementary Fig. S1a**). In all cases, DHQ III FFQ was administered prior to initiation of systemic therapy in person by a trained provider.

To evaluate impact of pre-treatment non-nutritive sweeteners (NNS) intake upon ICI efficacy, we determined the weight-normalized intake levels of sucralose and other NNS (aspartame, acesulfame, saccharin) relative to US FDA acceptable daily intake (ADI) levels and evaluated impact of sucralose intake upon ICI treatment outcomes including investigator-assessed objective response rate (ORR) and PFS (advanced melanoma and NSCLC) or major pathologic response (MPR) and relapse-free survival (high-risk resectable melanoma) (**Supplementary Fig. S1b and Supplementary Tables S1-4**). No significant demographic differences were observed between groups, and details regarding baseline demographics, concomitant medication and dietary intake, and treatment exposures are summarized in **Supplementary Fig. S1c**.

Daily NNS intake was dichotomized using a *cutpointr*-defined cutpoint (sucralose, 0.16mg/kg/d; acesulfame, 0.10mg/kg/d) across cohorts (**Fig. 1a, Supplementary Figs S2a-c**) (29). We observed that a high daily intake of sucralose (>0.16mg/kg/day) was associated with a trend towards lower ORR in ICI treated melanoma (**Fig. 1b**) and a significantly lower ORR in ICI-treated NSCLC (**Fig. 1c**). Commensurately, high sucralose intake (>0.16mg/kg/day) was significantly associated with poorer PFS in both ICI-treated advanced cutaneous melanoma (median 13.0 vs. 8.0 months, log-rank P = 0.037) and NSCLC (median 18.0 vs. 7.0 months, log-rank P = 0.034) (**Fig. 1d, e**). High sucralose intake was independently associated with low probability of ORR in ICI-treated advanced cutaneous melanoma [odds ratio 0.28 (0.085, 0.924), p = 0.0366] in a multivariate model after correcting for potential confounders (**Supplementary Table S1**). High sucralose intake was independently predictive of poorer PFS in ICI-treated melanoma in both univariate [hazard ratio 2.21 (1.02, 4.79), p = 0.0449] and multivariate [hazard ratio 2.91 (1.22, 6.96), p = 0.0164] models (**Supplementary Table S4a**). High sucralose intake had a similarly adverse impact upon ORR (**Supplementary Table S2**) and PFS (**Fig. 1b-c and Supplementary Table S4b**) in ICI-treated NSCLC.

Additionally, in an independent cohort of high-risk resectable melanoma patients treated with anti-PD-1 and a TLR9 agonist, high sucralose intake was associated with a significantly lower probability of major pathologic response (**Fig. 1f**) and lower RFS (median 25.0 vs. 19.0 months, log-rank *P* = 0.012) (**Fig. 1g and Supplementary Tables S3 and S4c**).

High daily intake of acesulfame (>0.10mg/kg/day) had a similar trend towards lower ORR and poorer PFS in ICI-treated melanoma and NSCLC as well as lower MPR and RFS in high risk resectable melanoma treated with ICI and TLR9 agonist (**Supplementary Figs. S2d-l**). There was no significant effect of high intake of other NNS evaluated including aspartame and saccharin upon ORR, PFS, or RFS (**Supplementary Figs. S3a-l**) except between aspartame intake and reduced MPR in high risk resectable melanoma (**Supplementary Fig. S3c**).

In order to dissect potential mechanisms of resistance as a result of sucralose consumption, we utilized two mouse models of cancer: MC38 (adenocarcinoma) and B16 (melanoma). Mice were exposed to a physiologically equivalent dose of sucralose (0.09mg/mL, ~0.45mg/day) based on their increased basal metabolic rates compared to humans(30) in the drinking water starting 2 weeks before tumor injection and were maintained on sucralose-containing water for the duration of treatment with anti-PD-1 (days 9, 12, 15) (**Fig. 2a**). Similar to our findings in anti-PD-1 treated NSCLC and melanoma patients, mice consuming sucralose were resistant to PD1-blockade in both MC38 (circles) and B16 (squares) and had significantly increased tumor growth, less $CD8^+$ T cell infiltration, and reduced survival across multiple tumor models (**Fig. 2b-d** and **Supplementary Fig. S4a-e**). Conversely, consumption of sucrose (table sugar) had no negative impact on response to anti-PD-1 (**Fig. 2b**). Tumor growth kinetics differed between mice sourced from Taconic (filled circles) compared to Jackson Labs (open circles) (**Fig. 2c** and **Supplementary Fig. S4b**), which house genetically identical mice with significantly distinct gut microbiomes (31,32). Additionally, tumor burden and size were significantly increased in sucralose-consuming mice after AOM-DSS driven colorectal cancer; however, this increase was only observable in mice sourced from Taconic, not those from Jackson (**Fig. 2d-e**). Further, cohousing of mice sourced from Jackson and Taconic reduced source effects on tumor growth (**Supplementary Fig. S4f-g**), suggesting a potential microbiome effect; therefore, we focused downstream

analyses on Taconic mice. Taken together, these data suggest that consumption of NNS prior to or during immunotherapy contributes to immunotherapy resistance in both mouse models and cancer patients.

Sucralose alters the tumor microenvironment via dysregulation of T cell function.

In order to determine how sucralose impacts the tumor microenvironment, we performed single cell RNA sequencing (scRNA-seq) on 76,804 cells isolated from the tumors (41,850 cells) and tumor draining lymph nodes (dLN) (34,954 cells) of sucralose-consuming anti-PD-1 treated Taconic mice. We identified seven clusters in the dLN and five clusters in the tumor that were annotated using marker genes (**Fig. 3a-b**). An unsupervised visualization indicated clear differences in the global transcriptomic profiles of both tumor and dLN cells from anti-PD-1 treated mice with and without sucralose treatment (**Fig. 3a-b**). To better dissect these differences, we used a novel supervised latent factor regression approach, SLIDE (Significant Latent Factor Interaction Discovery and Exploration) to identify latent factors that likely drive immunotherapy resistance during sucralose consumption (33) (**Supplementary Fig. S5**). Its unique statistical properties enable SLIDE to move beyond simple biomarkers to actual inference of the basis of immunotherapy resistance. Leveraging transcript abundances solely of $CD8^+$ T cells in the dLN, the SLIDE model provided significant discrimination between cells with and without sucralose treatment and it converged on 3 significant latent factors (context-specific co-expression modules) underlying altered $CD8^+$ T cell phenotype and function (**Supplementary Fig. S5a-j**). These three latent factors contained gene signatures associated with proliferative and functional stunting (downregulation of *Cdk8, Actb, Pfn1*) (34–36) and severe dysregulation or potentially exhaustion (including downregulation of *Il2rg* and upregulation of *Rps28* and *Rpl38*) (37),(38) found within the mice consuming sucralose (**Fig. 3c-d**). Interestingly, $CD4^+$ T_{conv} cells in the dLN were similarly affected and independently provided significant discrimination between the two groups (**Supplementary Fig. S5d-e**). While regulatory T cells (T_{regs}) also had distinctly altered transcriptomic profiles, the corresponding significant latent factors were suggestive of increased suppressive and functional

capacity (*Ctla4, Il2ra*, etc) (**Supplementary Fig. S5f**) (39–42). Separate SLIDE models were also built using transcript abundances within the tumor compartment. We identified three significant latent factors within the $CD8^+$ T cell compartment, most of which suggested metabolic stress and exhaustion (*Sirpa, Apoe, Nrf2*, etc) and provided clear discrimination between groups (**Supplementary Fig. S5g-j**) (43–45). Interestingly, changes in the $CD4^+$ T_{conv} subset within the tumor were far less discriminative than those in the dLN, likely reflective of the known predominant role of $CD8^+$ T cells in mediating antitumor immunity, and corresponding immunotherapy resistance upon sucralose treatment (**Supplementary Fig. S5k-n**). Further analysis of $CD8^+$ T cells from the tumor and dLN of sucralose+anti-PD-1 mice showed an increase in T cell exhaustion signatures, including increases in *Pdcd1*, *Tox*, *Lag3*, *Tigit*, *Icos*, *Ctla4*, and *Prf1* as well as downregulation of some solute carrier family members (SLCs), including those that transport glucose (*Slc2a3*, *Slc2a1*) and those required for mitochondrial respiration (*Slc25a36*, *Slc25a19*) (**Fig. 3c-d and Supplementary Fig. S6a-e**).

When assessed at the protein level, both $CD8^+$ T cells and $CD4^+$ T_{conv} cells displayed signs of reduced T cell cytotoxic function, including a significant reduction in total mitochondrial mass (**Fig. 3e**), reduced TCF1:Tox ratios (**Supplementary Fig. S7a**) and reduced polyfunctionality as shown by TNFα and IFNγ (**Fig. 3f**) (37). No significant differences in cell number were noted; however, the activation status of T cells was significantly altered, especially in the dLN of sucralose consuming mice (**Supplementary Fig. S7b-d**). We next sought to determine whether sucralose-driven T cell dysfunction was unique to the tumor microenvironment. We infected mice consuming sucralose with LCMV cl-13 prior to treatment with anti-PD-1. Sucralose consuming mice experienced more severe disease and an increase of T cell exhaustion, especially in $gp33^+$ LCMV-specific $CD8^+$ T cells (**Supplementary Fig. S7e-l**), suggesting that sucralose effects on T cell function were not restricted to cancer, but rather may contribute to overall T cell dysfunction across disease states ranging from cancer to chronic viral infection.

We next performed a series of *in vitro* assays to determine whether sucralose could have a direct effect on T cell function and whether the timing of sucralose exposure affected T cell function. $CD8^+$ T cells expanded in sucralose-supplemented media

proliferated slower than untreated controls (**Supplementary Figs. S8a-b**). Further, $CD8^+$ T cells had increased apoptosis as measured by Annexin V after 20-hour exposure to a downstream microbial metabolite, sucralose-6-acetate (**Supplementary Fig. S8c**). T cells cultured in sucralose were moderately less functional as shown through reduced Granzyme B expression and reduced ability to kill target cells *in vitro* (**Supplementary Fig. S8d-f**). Additionally, T cells expanded for 7 days in sucralose (in the absence of persistent antigen) showed moderate signs of metabolic exhaustion with reduced mitochondrial mass (**Supplementary Fig. S8g**); however, other markers of T cell exhaustion such as PD-1, Tox, oxidative respiration, and glycolysis were not impacted (**Supplementary Fig. S8h-o** and **S9a-d**). There were no observable differences in proximal TCR signaling (**Supplementary Fig. S10**). RNA-seq of T cells exposed to sucralose *in vitro* for 7 days showed shifts in metabolic pathways, including downregulation of amino acid metabolism (*Slc7a3*), TCA cycle, and glycolysis. (**Supplementary Fig. S11a-b**). While some of the macroscopic transcriptional properties identified *in vitro* readouts mimicked those found directly *ex vivo* (decreased cell killing, metabolic rates), there was only mild overlap between *in vitro* and *ex vivo* analyses, suggesting that the host environment is critical for sucralose-driven T cell dysfunction. Taken together, these data suggest that sucralose consumption has deleterious effects across multiple T cell processes, including proliferation, cytotoxic function, and metabolism, but that the severity of T cell dysfunction is dependent upon the host factors, most notably the microbiome.

The gut microbiome is necessary and sufficient to limit immunotherapy response after sucralose consumption.

ICI response in cancer patients is associated with select members of the gut microbiome(46)(47)(48)(49)(50). We observed that mice sourced from different vendors (harboring distinct microbiomes) varied in their response to anti-PD-1 upon consuming sucralose (**Fig. 2c-e**). Therefore, we hypothesized that the gut microbiome may be responsible for T cell dysfunction and ICI resistance in the presence of sucralose. Therefore, we subjected mice to sucralose as before with the addition of select antibiotics, including vancomycin, ampicillin, or broad-spectrum antibiotics (MANV—

metronidazole, ampicillin, neomycin, vancomycin) (**Fig. 4a**). Interestingly, while ampicillin had no impact on tumor growth during sucralose consumption (complete response [CR]: 20%), vancomycin, a bacteriostatic antibiotic that targets gram positive bacteria (CR: 44%) increased overall response rates in mice consuming sucralose and receiving anti-PD-1 (**Fig. 4b**), suggesting that the gut microbiome may be associated with sucralose-driven resistance to anti-PD-1. To determine whether the gut microbiota was sufficient to drive ICI resistance after sucralose consumption, we performed fecal microbial transfers (FMT) from sucralose-consuming donor mice to sucralose-naïve mice prior to injecting tumors and treating with anti-PD-1 (**Fig. 4c**). Strikingly, FMTs from sucralose-consuming mice phenocopied direct consumption of sucralose in both tumor progression and overall survival (**Fig. 4d**). Therapeutic FMTs from responder patients or healthy donors have shown great promise as a therapeutic option in conjunction with anti-PD-1 to patients with resistant or refractory melanomas (51),(52). Therefore, we sought to determine whether sucralose-driven resistance could be overcome with an FMT therapeutically. Indeed, immune checkpoint inhibitor (ICI) resistance of sucralose-consuming mice was reversible by performing an FMT from anti-PD-1 responder mice, with the most significant benefit shown in those that were prepped with antibiotics before the FMT suggesting that removal of sucralose-associated bacteria was required for response to anti-PD-1 (**Fig. 5a-c**).

In order to determine how the gut microbiome is contributing to sucralose-driven resistance, we performed shallow shotgun metagenomic sequencing on serial stool samples of mice consuming sucralose and receiving anti-PD-1. Interestingly, sucralose significantly shifted the gut microbiome, regardless of anti-PD-1 treatment (**Fig. 6a-b, Supplementary Fig. S12a-b**). Alpha diversity and evenness were reduced in both sucralose and sucralose + anti-PD-1 treated groups compared to controls, although this was not significant (**Supplementary Fig. S12c and S13a**). Specifically, we observed increases in *Firmicutes* and *Proteobacteria* phyla, with a relative outgrowth of select gram-positive bacteria, including *Clostridiaceae* and *Lachnospiraceae* after sucralose consumption (**Fig. 6c and Supplementary Fig. S13b**). Thus, these data would suggest that ICI resistance after sucralose consumption is possibly due to phenotypic or functional shifts in the gut microbiota and is associated with an outgrowth of gram-positive bacteria.

Arginine supplementation during sucralose consumption restores T cell function and immunotherapy efficacy.

In order to assess how the gut microbiota was functionally impacted by sucralose consumption, we further analyzed the functional characteristics from stool samples through both metagenomics and untargeted/targeted metabolomics. Through further pathway analysis, we found several significantly altered pathways involving amino acids (**Fig. 6d**). Upon further investigation, we identified an increase in enzymes associated with arginine degradation pathways (**Fig. 6e**). Metabolomics of stool samples showed that sucralose and its microbial metabolite, Sucralose-6-Acetate, were only found within stool samples from mice consuming sucralose in the drinking water as expected (**Supplementary Fig. S13c**). Pathway analysis of untargeted stool metabolomics revealed that a number of pathways were enriched due to sucralose consumption during anti-PD-1 treatment, including arginine degradation (**Fig. 7a**). Indeed, levels of arginine, as well as many associated metabolites (citrulline), were significantly reduced in the stool of sucralose consuming mice (**Supplementary Fig. S13d**), while other metabolites were unaffected (**Supplementary Fig. S13e**), suggesting a potential role for arginine degradation after sucralose consumption. Upon further analysis, we also found that arginine levels in the sucralose+anti-PD-1 group were significantly reduced in both the serum and tumor interstitial fluid (TIF) (**Fig 7b-c**). Additionally, we found that sucralose exposure led to a reduction in the amino acid transporter, *Slc7a3*, which is responsible for arginine uptake (**Supplementary Fig. S11a**). Arginine is a key metabolite required for optimal T cell metabolism and function, and it has been previously associated with cytotoxic T cell function in cancer (53). To test the possibility that a reduction in arginine was responsible for ICI resistance, we supplemented sucralose-containing drinking water with arginine (3.75 mg/mL) or citrulline (3.75 mg/mL), the latter of which has been shown to lead to the highest levels of serum arginine *in vivo* (**Fig. 7d**) (54) (55). Metabolomics of the serum and TIF revealed that citrulline could restore levels of arginine in both sites to that of anti-PD-1 treated mice (**Fig. 7c**). In addition, both $CD4^+$ and $CD8^+$ T cells from arginine or citrulline fed mice displayed enhanced function shown by an increase in IFNγ production in the tumor, with

the biggest increase found in citrulline treated groups (**Fig. 7e**). Quite strikingly, supplementation with citrulline restored response to anti-PD-1 even in the presence of sucralose and led to an overall survival advantage (**Fig. 7f-h** and **Supplementary Fig. S13f**). Taken together, these data suggest that sucralose shifts the gut microbiota in a way that reduces arginine levels and ultimately drives resistance to anti-PD-1.

Discussion

The gut microbiota composition has been directly correlated with ICI response in multiple cancers including melanoma and NSCLC (10,11,13,14,46,47,56). Development of therapeutic strategies to shift the gut microbiota are underway through use of probiotics, FMT, and dietary interventions. Certain diets, including those high in fiber and fermented foods, can significantly alter the diversity and makeup of gut microbiota, and consequently alter immunological outcomes in healthy volunteers and ICI-treated cancer patients(57,58). While various dietary elements such as dietary fiber augment ICI efficacy by favorably modulating gut microbiome, how other dietary elements including NNS intake affect ICI efficacy is unknown. Our work suggests that increased sucralose consumption is associated with poorer efficacy of ICI based immunotherapy in melanoma and NSCLC patients, and sheds light on how sucralose may impact T cell functionality and ICI efficacy in a gut microbiome-centric fashion. Future prospective studies will be necessary to assess potential causation of sucralose in driving immunotherapy resistance as well as to determine how other demographic factors, including location and food access, may impact overall responses.

NNS use has increased significantly over the last 50 years in an attempt to reduce table sugar consumption. Given that most NNS are low or zero calorie, these have traditionally been overlooked as contributing factors to overall health and disease. Multiple NNS, including sucralose, saccharin, and others, have recently been shown to reduce microbial diversity and lead to glucose intolerance in healthy hosts(12,24,59). Interestingly, sucralose has been associated with poor T cell function in multiple disease states when supraphysiological amounts are consumed, suggested a potential immunosuppressive mechanism of some NNS such as sucralose. How NNS may contribute to cancer progression and immunotherapy response remained unknown.

Our results show that increased high pre-treatment sucralose intake was associated with lower PFS in advanced cutaneous melanoma and NSCLC patients treated with PD-1 based ICI regimens, and lower RFS high-risk resectable melanoma patients treated with anti-PD1 and TLR9 agonist, hinting at the ability of sucralose to blunt efficacy of ICI immunotherapy regardless of histology or stage. Preclinical studies of melanoma and carcinogen induced colorectal cancer suggested that sucralose consumption drove poor response to checkpoint inhibitors through microbial dysbiosis and downstream $CD8^+$ T cell dysfunction, a fundamental but not well understood mechanism of ICI resistance. Given that this is limited to two tumor models in mice, further analysis of other cancer types and immunotherapy modalities may provide more insight into the broad implications of sucralose consumption. While sucralose may have some effects directly upon T cell activation (**Supplementary Fig. S8**)(27), our data suggests that sucralose consumption interacts directly with gut microbiota to diminish sensitivity to anti-PD-1 therapy, and are both necessary and sufficient to drive degradation of key amino acids, $CD8^+$ T cell dysfunction, increased tumor growth, and reduced response to anti-PD-1. These results are in line with prior observations regarding the host-specific microbiome-dependent metabolic alterations observed in patients treated with sucralose(25). Therefore, dietary effects on the microbiota may represent a previously unappreciated mechanism of resistance to checkpoint blockade in melanoma or other cancer types. Further, our study bolsters the growing notion that artificial non-nutritive sweeteners, even those manufactured from sugar like sucralose, are not inert and can have broad immunomodulatory effects that adversely affect patient outcomes. Our results suggest that select metabolites that are regulated by the gut microbiota may be required for ICI response and may represent a fundamental component of anti-tumor immunity.

METHODS

Patient samples

Human study subjects – HCC 20-019

This study includes dietary history data from advanced cancer patients treated with anti-PD-1 based immune checkpoint inhibitor (ICI) therapy evaluated at the UPMC Hillman Cancer Center (UPMC HCC) in Pittsburgh, PA. All patients provided voluntary written informed consent to research procedures, including biospecimen collection, under Institutional Review Board (IRB) approved protocol HCC 20-019 (Comprehensive Intestinal Microbiome and Dietary History Evaluation of Patients with Advanced Cancers on Treatment with Immune Checkpoint Blockade, IRB approval number MOD20010266-016). All studies included were conducted in accordance with recognized ethical guidelines as applicable (Declaration of Helsinki, CIOMS, Belmont Report, US Common Rule).

Specifically, we included patients who had received systemic anti-PD-1 based immunotherapy or chemoimmunotherapy between September 2020 and June 2024. Eligible patients had received systemic anti-PD-1 based immunotherapy or chemoimmunotherapy for advanced/metastatic melanoma or non-small cell lung cancer (NSCLC) as part of standard treatment (outside of a clinical trial), had undergone dietary history evaluation using Diet History Questionnaire III (DHQ III), had received treatment for at least 3 months, had at least 1 post-treatment imaging study evaluable for response and had adequate follow up time (6 months) following initiation to therapy. Radiographic response to therapy was determined by the investigators providing the clinical treatment and assessed using response evaluation criteria in solid tumors (RECIST v1.1)(60). Clinical response to therapy was assessed at each visit. Progression was defined based on first documented clinical and/or radiographic progression and confirmed in all instances.

Overall, 132 patients with advanced cancer (melanoma = 91; NSCLC = 41) who received systemic PD-1 based immunotherapy singly or in combination with chemotherapy and met other criteria as above were included in the primary analysis of patient outcomes (**Supplementary Fig. 1**).

Human study subjects – HCC 17-169 (phase II trial of neoadjuvant nivolumab and TLR9 agonist vidutolimod in high-risk resectable melanoma)

This study includes dietary history data from patients who were enrolled in a prospective phase II trial of neoadjuvant nivolumab and TLR9 agonist vidutolimod in high-risk resectable melanoma, the primary results of which were previously reported (28). Briefly, this single-institution, non-randomized, investigator-initiated phase 2 study enrolled histologically proven clinical stage III cutaneous melanoma. Eligible patients received neoadjuvant intratumoral vidutolimod and systemic nivolumab prior to surgery. Patients received three doses of intravenous nivo (240 mg) every 2 weeks, together with seven weekly doses of vidu (5 mg subcutaneous on week 1; then 10 mg intratumoral on weeks 2–7). Following neoadjuvant treatment, patients underwent restaging imaging and proceeded to surgery. Following surgery, all patients adjuvant systemic nivolumab and subcutaneous vidutolimod.

The primary endpoint of the trial was major pathologic response (MPR) as assessed using consensus criteria(61–63). A key secondary endpoint was relapse-free survival (RFS), defined as time from surgery to disease recurrence or death from any cause. Briefly 34 patients were enrolled, but 3 withdrew consent, and hence 31 were evaluable for safety, while 30 were evaluable for pathologic response (1 patient had systemic disease progression after neoadjuvant therapy precluding surgery). DHQ III data was available on 25 of the 31 enrolled patients.

Clinicodemographic variables.

Body mass index, NLR and lactate dehydrogenase were based on values obtained immediately before therapy or on the day of ICI therapy initiation. Tumor-specific characteristics including TMB and PD-L1 status was abstracted from the electronic record.

Survival endpoints.

PFS was defined as the time from the start of therapy to first confirmed clinical and/or radiographic progression. RFS was defined as time from surgery to disease recurrence or death from any cause. Patients were censored as of the date of last contact.

Assessment of dietary data

Dietary intake data was collected using the DHQ III, a standardized and validated tool for nutritional assessment developed by the National Cancer Institute's (NCI) Division of Cancer Control and Population Sciences (DCCPS). The DHQIII was designed based on a compilation of national 24-hour dietary recall data from the National Health and Nutrition Examination Surveys (NHANES) conducted in 2007-2014(64). We utilized the "past month with portion size" DHQ III FFQ version, and this was self-administered via a web-based portal using a tablet to patients within 3 weeks of them starting ICI therapy. To facilitate dietary data intake by patients who may not be comfortable with self-administered questionnaires, administration was proctored by trained research coordinators. Responses to all 135 questions are converted to daily frequencies

The DHQ III consists of 135 food and beverage line items and 26 dietary supplement questions. Some line items for foods and beverages have additional embedded questions that allow for final assignment to items in the nutrient and food group database leading to 263 foods/beverages listed in the database. For example, a single line item asks frequency of intake and portion size of soda or soft drinks. Embedded underneath are questions regarding whether the soft drinks consumed are regular vs. diet or caffeinated vs. decaffeinated. Answers to these questions lead to assignment of one of four food codes in the database: diet soda with caffeine, diet soda without caffeine, regular soda with caffeine or regular soda without caffeine. The questions pertaining to NNS intake are listed on the left.

Overall, the DHQ III FFQ permits estimation of each patient's daily dietary intake of any particular nutrient, macronutrient or vitamin as an average over the previous month. Correlation between DHQ III and 24-hour recall studies have been previously published(65).

All patients who completed a DHQ III were included in the analysis, but those who did not complete the entire questionnaire, had received <3 months of ICI therapy, or were found to consume <1000kcal/day (suggestive of inaccurate reporting) were excluded. DHQ III output including non-nutritive sweeteners (NNS) intake as an average daily intake of mg/day. NNS dietary data was normalized by taking each patient's respective NNS intake (mg/day) and dividing by their weight (kg) to have a weight-normalized average daily intake (ADI) of mg/kg/day. The weight-normalized ADI could then be

compared to the FDA's acceptable daily intake (ADI) limit, previously reported for the various NNS: sucralose (5mg/kg/day), aspartame (50mg/kg/day), acesulfame (15mg/kg/day), and saccharin (15mg/kg/day).

Statistical methods

To evaluate sucralose (and other NNS) thresholds, we utilized CutpointR(29) which robustly estimates the optimal cutpoint in any given distribution. The CutpointR-defined threshold for any given NNS was used to dichotomize that cohort. Kaplan Meier survival analysis was performed with StataSE, using the optimal cutpoint determined by CutpointR with the minimize_metric, to define the association of high or low NNS intake with ORR or PFS. Chi-square test was used to compare the investigator-assessed objective response rates (ORR) between high and low intake groups.

Univariate and multivariate analyses were performed by a PhD biostatistician (H.W.) to investigate the association of normalized sucralose intake and other covariables with PFS (or RFS) and ORR (or MPR). The covariables assessed include gender, BMI, pre-treatment neutrophil:lymphocyte ratio (NLR), pre-treatment lactate dehydrogenase (LDH), soluble dietary fiber intake (g/day), insoluble dietary fiber intake (g/day), hypertension, and heart disease status. We also assessed effect of combination vs. single-agent ICI therapy (melanoma patients only); and the effects of chemoimmunotherapy vs. single-agent ICI therapy, TMB (continuous variable) and PD-L1 status (1% vs. >1%) in NSCLC patients only.

Univariate logistic regression models were used to test the association of ORR (or MPR) with each variable. We used the stepwise model selection procedure to build a multivariate logistic regression model where high sucralose intake (>0.16mg/kg/day) was forced in the model. In this procedure, we started from a univariate model with high sucralose intake (>0.16mg/kg/day). Then, at each step along the way we either entered or removed a predictor based on the chi-square test p-value for the effect of this predictor in the multivariate model. We stopped when no more predictors could be justifiably entered or removed from our stepwise model, thereby leading us to a final model. We set a significance level for deciding when to enter a predictor into the stepwise model and a significance level for deciding when to remove a predictor from the model. We set the two significance levels to be 0.35 and 0.10 respectively.

Advanced melanoma, advanced NSCLC and neoadjuvant melanoma patients were analyzed using separate univariate logistic regression models.

To test the association of PFS (or RFS) with each variable, a univariate Cox model was used. Advanced melanoma, advanced NSCLC and neoadjuvant melanoma patients were analyzed using separate univariate Cox models.

The data were analyzed in SAS Version 9.4 (SAS Institute Inc., Cary, NC).

In vitro T cell cultures

Spleen and lymph nodes were isolated from C57BL/6-Tg(TcraTcrb)1100Mjb/J mice (RRID: IMSR_JAX:003831). Cells were activated in complete RPMI-1640 (Gibco: 11875119) supplemented with 10% Fetal Bovine Serum (FBS) (Gibco: 16000069), 250ng/mL SIINFEKL peptide (Genscript: RP10611), and 50U/mL IL-2 (Peprotech: 212-12). Cells were activated for 24 hours, and then cells were washed and cultured for 6 additional days in RPMI-1640 supplemented with 50U/mL of complete RPMI supplemented with FBS. For in vitro sucralose treatment, control complete RPMI-1640 was supplemented with 0.22g/L sucralose, and 10-fold dilutions were made using complete RPMI.

Flow cytometry:

Tumor draining lymph nodes (tdLN), nondraining lymph nodes (ndLN), spleens, and tumors were harvested in 10% complete RPMI-1640 at day 14 post tumor injection. Tumors were also harvested with DNAse I and Liberase TL for digestion. Tissues were processed through a 70uM strainer to obtain single cell suspension. Single cell suspensions were stained with live/dead and required surface markers for 15 minutes on ice, then fixed with either eBiosciences Foxp3 Transcription Factor (for intracellular transcription factor analysis) reagents or BD CytoFix (for intracellular cytokine analysis) reagents prior to staining intracellular markers for 45 minutes on ice.

Single cell suspensions were stimulated with phorbol 12-myristate 13-acetate (PMA), ionomycin, and brefeldin A for 2.5 hours at 37C prior to staining and fixation for flow cytometry analysis. After stimulation, single cell suspensions were stained as described above.

Flow analysis was performed on a Cytoflex (Beckman Coulter) cytometer or a Fortessa (Beckman Dickinson) cytometer. All experiments were analyzed using FlowJo Software (v10.9). Cells from tumors, spleens, and lymph nodes were isolated, resuspended in PBS, and placed on ice. Surface markers were stained with fluorescently conjugated antibodies for 30 minutes on ice. All flow analysis included size exclusion (FSC x SSC), and doublet exclusion (FSC-Height/FSC-Area). Zombie Dye Viability Kits (Biolegend) or Live/Dead Fixable Aqua Stain Kits (ThermoFisher) were used to distinguish live and dead cells, and positive dead cells were excluded from analysis. Antibodies were purchased from ThermoFisher Invitrogen, BioLegend, Beckman Dickinson (BD), Cell Signaling, and R&D Systems.

The following antibodies were used: IL-2 Pe-Cy7 (BD Pharmingen 560538, RRID:AB_1727545), IFNγ Af647 (Biolegend 505816, RRID:AB_493314), Granzyme B – FITC (Biolegend: 515403, RRID:AB_2114575), TNF – PerCPCy5.5 (Biolegend 506322, RRID:AB_961435), Tcf1 – Af488 (Cell Signaling: 6444S, RRID:AB_2797627), PD-1 – BV785 (Biolegend 135225, RRID:AB_2563680), Tim3- BV421 (Biolegend 119723, RRID:AB_2616908), CD44 – PerCPCy5.5 (Biolegend 103032, RRID:AB_2076206), CD73 – APC (Biolegend 127210, RRID:AB_11219400), CD39 – PE-Cy7 (Biolegend 143806, RRID:AB_2563393), Tox – APC (eBioscience 50-6502-82, RRID:AB_2574265), CD8a – PE (Biolegend 100707, RRID:AB_312747), CD8a - Pe-Cy7 (Biolegened 100721, RRID:AB_312760), IFN γ – eFluor450 (Invitrogen 48-7311-82, RRID:AB_1834366), CD8b – BV786 (BD OptiBuild 740952, RRID:AB_2740577), CD4 – PE-Cy7 (BD Pharmingen 552775, RRID:AB_394461) TCR β – PerCP-Cy5.5 (Invitrogen 45-5961-82, RRID:AB_925763), IL-17A – APC (Invitrogen 17-7177-81, RRID:AB_763580), TNF α – AF700 (Biolegend 506338, RRID:AB_2562918), CD62L – BV785 (Biolegend 104440, RRID:AB_2629685), LAG-3 – PerCP-Cy5.5 (Biolegend 125212, RRID:AB_2561517), Tim-3 – PE (Biolegend 119703, RRID:AB_345377), CD8a – BUV737 (BD Horizon 612759, RRID:AB_2870090), TCF7/TCF1 – AF488 (R&D Systems IC8224G, RRID:AB_3656680), CD19 – eFluor450 (Invitrogen 48-0193-82, RRID:AB_2734905), FOXP3 – AF488 (Invitrogen 53-5773-82, RRID:AB_763537), CD44 – PE-Cy7 (Invitrogen 25-0441-82, RRID:AB_469623), TOX – eFluor660 (Invitrogen 50-6502-82, RRID:AB_2574265), CD4 – APC

(Invitrogen 17-0042-82, RRID:AB_469323), Rpl18 Tetramer – PE (NIH Tetramer Facility), Rpl18 Tetramer – APC (NIH Tetramer Facility).

Metabolic labelling for flow cytometry

For metabolic staining, neutral lipids were labeled using 1.9µM Bodipy 493/503 (Thermo: D3922) in PBS for 30 minutes at 37˚ C. Glucose uptake was measured using Glucose-Cy3. Single cell suspensions of ~1 million cells/mL were placed in serum-free RPMI-1640 containing 0.4µM Glucose-Cy3 for 30 minutes at 37˚ C. Mitochondrial mass was determined using 10nM Mitotracker Deep Red FM (Thermo: M22426) or MitoTracker Green (Thermo: M7514). Cells were labeled with Mitotracker on ice for 30 minutes. Mitochondrial membrane potential was measured using tetramethylrhodamine (TMRE). Cells were resuspended with PBS supplemented with 20nM TMRE just prior to running on the cytometer, and cell suspensions were run directly on the cytometer. All metabolic labeling was conducted on live cells, and these samples were not fixed prior to running on the cytometer.

Extracellular Flux Analysis

Isolated T cells were plated on PDL-Coated Cell Culture Microplates (Agilent 103799-100) in unbuffered Seahorse XF RPMI assay medium supplemented with 2mM glutamine, 1mM sodium pyruvate, and 10mM glucose. OCR and ECAR were measured in an Agilent Seahorse XFe96 extracelluar flux analyzer. During the assay, cells received four separate injections of 1) 2µM Oligomycin, 2) 2µM FCCP, 3) 10mM 2-DG, 4) and 0.5µM Rotenone and 0.5µM Antimycin A were used.

xCELLigene real-time killing assay:

15,000 B16_OVA cells were seeded onto the E-Plate VIEW 96 (Agilent 300601020) and incubated for a minimum of 5 hours. Subsequently, primary CD8 T cells, isolated from C57BL/6-Tg(TcraTcrb)1100Mjb/J (Strain #:003831, common name: OT1), were introduced to the E-Plate 96 at various Effector (E) to target (T) ratios. Following this, the system was left undisturbed for a minimum of 18 hours to allow the Agilent xCELLigence RTCA DP system to record impedance changes. The RTCA Software Pro was utilized for cytolysis calculations.

Western Blot

CD8 T cells were magnetically enriched from splenocytes derived from C57BL/6J Mice. After isolation, cells were resuspended in control serum-free RPMI, or serum-free RPMI supplemented with 2% Splenda or 0.22g/L sucralose and stimulated with 3µg/mL biotin-labeled αCD3 antibody, 4µg/mL of αCD28 antibody, and + 1.5µg/mL streptavidin for the indicated times: 5 minutes, 15 minutes, 30 minutes, or left unstimulated (0 min) at 37oC. After stimulation, cells were lysed, and western blots were conducted using the following antibodies: Phospho-Akt (Ser473) (D9E) XP® Rabbit mAb #4060, Akt (pan) (C67E7) Rabbit mAb #4691, mTOR Antibody #2972, Phospho-mTOR (Ser2448) Antibody #2971, PLCγ1 (D9H10) XP® Rabbit mAb #5690, Phospho-PLCγ1 (Ser1248) (D25A9) Rabbit mAb #8713, Zap-70 (D1C10E) XP® Rabbit mAb #3165, Phospho-Zap-70 (Tyr319)/Syk (Tyr352) Antibody #2701, p70 S6 Kinase (49D7) Rabbit mAb #2708, Phospho-p70 S6 Kinase (Thr389) Antibody #9205, Lck Antibody #2752, Phospho-Lck (Tyr505) Antibody #2751, p44/42 MAPK (Erk1/2) (137F5) Rabbit mAb #4695, Phospho-p44/42 MAPK (Erk1/2) (Thr202/Tyr204) Antibody #9101.

Flow Cytometry Single Cell Suspensions and Staining

Tumor draining lymph nodes (tdLN), nondraining lymph nodes (ndLN), spleens, and tumors were harvested in 10% complete RPMI-1640 at day 14 post tumor injection. Tumors were also harvested with DNAse I and Liberase TL for digestion. Tissues were processed through a 70uM strainer to obtain single cell suspension. Single cell suspensions were stained with live/dead and required surface markers for 15 minutes on ice, then fixed with either eBiosciences Foxp3 Transcription Factor (for intracellular transcription factor analysis) reagents or BD CytoFix (for intracellular cytokine analysis) reagents prior to staining intracellular markers for 45 minutes on ice.

Single cell suspensions were stimulated with phorbol 12-myristate 13-acetate (PMA), ionomycin, and brefeldin A for 2.5 hours at 37C prior to staining and fixation for flow cytometry analysis. After stimulation, single cell suspensions were stained as described above.

Mice

Female 6-week-old C57Bl/6 mice were obtained from Jackson Laboratories and Taconic Biosciences. All animal experiments were performed in the American Association for the Accreditation of Laboratory Animal Care-accredited specific-pathogen-free facilities in the Division of Laboratory Animal Resources at the University of Pittsburgh School of Medicine (UPSOM). All animal protocols were approved by the Institutional Animal Care and Use Committees of the University of Pittsburgh. Mice in the same group were cohoused unless otherwise stated.

C57Bl/6 mice sourced from both Jackson and Taconic were given approximately 24 hours to acclimate to the BSL2 animal facility prior to starting treatment with sucralose. All mice were always kept in immunocompromised housing conditions. All Jackson sourced mice were handled prior to handling any Taconic sourced mice. Full disinfection of all surfaces by lab staff was performed between Jackson and Taconic mice to minimize cross contamination. In cohousing experiments, Jackson and Taconic sources C57Bl/6 mice were mixed into cages equally and lab staff took care in disinfecting all surfaces and tools in between cages. Mice were always handled in the order of: Jackson, Taconic, and cohoused mice with disinfection between each group.

Sucralose Supplementation

400 mL bottles of sterilized water were spiked with 36 mg sucralose (Sigma Aldrich), equivalent to 3 packets of sucralose containing non-nutritive sweetener. Based on differing basal metabolic rates and surface area between mice and humans, we estimate that mice consuming 18.75mg/kg/day sucralose is roughly equivalent to humans consuming 1.458mg/kg/day (ADI is 5mg/kg/day) based on the previously calculated equation, whereby the reference body weight is 0.02kg for mice and 60kg for humans:

(animal dose) x (y) = Human Equivalent Dose (HED) *y=0.081 mouse to human*

(18mg/kg) x (0.081) = 1.458mg/kg/day

Bottles were replaced every 7-10 days. Mice were consumed sucralose for 14 days prior to tumor cell injections and throughout the duration of the experiment or as noted.

For some experiments, water was also supplemented with either 3.75g/L arginine or citrulline for the duration of the experiment.

Murine Tumor Models

C57Bl/6 mice were injected with MC38 murine colorectal adenocarcinoma (2.5x10^5 cells subcutaneously) or B16 melanoma (1.25x10^5 intradermally). Cell lines were obtained from the Vignali Lab (University of Pittsburgh) and were tested as mycoplasma free by PCR in 2022. Cells were saved no later than passage 2 and were injected after 2 passages directly from freeze thaw. Tumors were measured every three days with calipers to calculate tumor area. Mice were randomly assigned to groups prior to tumor injection. 200 ug of anti-PD-1 (BioXCell) was injected intraperitoneally on days 9, 12, and 15 post tumor injection. Mice were marked as responders if tumor size decreased upon treatment with anti-PD-1. Complete responder (CR) was defined as total eradication of tumor, resulting in tumor area of zero.

To establish carcinogen-induced colorectal cancer in mice, we injected 10mg/kg Azoxymethane (AOM) i.p. on Day 0, prior to 3 cycles of a '1 week on, 2 weeks off' schedule of administering 3% DSS in the drinking water beginning on Day 7. Mouse weights were monitored weekly and euthanized if more than 25% weight was lost. Mice were sacrificed 12 post AOM, and tumors were enumerated and measured.

Fecal Microbiome Transplants

Female C57Bl/6 recipient mice were treated with broad spectrum antibiotics (metronidazole, ampicillin, neomycin, vancomycin) for seven days prior to transplant, unless otherwise noted. Stool pellets were collected from donor mice and mixed into 500 uL of sterile 1x phosphate buffered saline (PBS). The supernatant is then filtered through a 70 uM filter and transferred into a syringe with a murine feeding needle attached. 200 uL of the filtered supernatant is then orally gavaged into each mouse.

Antibiotic Depletion

Broad spectrum antibiotics were administered to mice through sterile tap drinking water spiked with metronidazole (0.5 g/L), ampicillin (1 g/L), neomycin (1 g/L), and vancomycin (1 g/L). Broad spectrum antibiotic mix was also sweetened sucralose as

described above. This was administered over 7 days and mice were monitored daily to ensure consumption.

Metabolomics: Untargeted High-Resolution LC-HRMS

Sample preparation-Mouse Stool

Taconic mice were given sucralose-containing or regular water for 14 days prior to tumor injection (MC38) and were maintained on the same water regimen for the remainder of the experiment. Mice were treated with 200ug anti-PD-1 on day 12, and stool, serum, and tumor interstitial fluid were collected 14 days after tumor injection.

To isolate tumor interstitial fluid, tumors were harvested into an empty 15mL conical tube on ice. A single slice was made in each tumor, penetrating 50% of the tissue to allow for better fluid extraction. Tumors were then placed on a 5uM nylon membrane in an empty Eppendorf or 15mL tube and spun at 3000rpm for 60 minutes at 4 degrees Celsius. Fluid was immediately collected and frozen at -80 degrees Celsius until analysis.

Metabolic quenching and polar metabolite pool extraction was performed by adding ice cold 80% methanol (aqueous) at a ratio of 1:15 wt input tissue:vol. (D_3)-creatinine, (D_4)-taurine, (D_3)-lactate and (D_3)-alanine (Sigma-Aldrich) were added to the sample lysates as an internal standard for a final concentration of 10µM. Samples are homogenized using a MP Bio FastPrep system using Matrix D (ceramic sphere) for 60 seconds at 60hz. The supernatant was then cleared of protein by centrifugation at 16,000xg. 2µL of cleared supernatant was subjected to online LC-MS analysis.

LC-HRMS Method

Analyses were performed by untargeted LC-HRMS. Briefly, Samples were injected via a Thermo Vanquish UHPLC and separated over a reversed phase Thermo HyperCarb porous graphite column (2.1×100mm, 3µm particle size) maintained at 55°C. For the 20 minute LC gradient, the mobile phase consisted of the following: solvent A (water / 0.1% FA) and solvent B (ACN / 0.1% FA). The gradient was the following: 0-1min

1% B, increase to 15%B over 5 minutes, continue increasing to 98%B over 5 minutes, hold at 98%B for five minutes, reequillibrate at 1%B for five minutes. The Thermo IDX tribrid mass spectrometer was operated in both positive and ion mode, scanning in ddMS^2 mode (2 µscans) from 70 to 800 m/z at 120,000 resolution with an AGC target of 2e5 for full scan, 2e4 for ms^2 scans using HCD fragmentation at stepped 15,35,50 collision energies. Source ionization setting was 3.0 and 2.4kV spray voltage respectively for positive and negative mode. Source gas parameters were 35 sheath gas, 12 auxiliary gas at 320°C, and 8 sweep gas. Calibration was performed prior to analysis using the Pierce™ FlexMix Ion Calibration Solutions (Thermo Fisher Scientific). Integrated peak areas were then extracted manually using Quan Browser (Thermo Fisher Xcalibur ver. 2.7). Untargeted differential comparisons were performed using Compound Discoverer 3.0 (Thermo Fisher) to generate a ranked list of significant compounds with tentative identifications from BioCyc, KEGG, and internal compound databases. Purified standards were then purchased and compared in retention time, m/z, along with ms2 fragmentation patterns to validate the identity of significant hits.

Stool Metabolomics: 3NP-Short Chain Fatty Acids and Tricarboxylic Acids

Sample Preparation

Mouse stool samples were homogenized with 50% aqueous acetonitrile at a ratio of 1:15 vol:wt. 5µg/mL Deuterated internal standards: (D_2)-formate, (D_4)-acetate, (D_5)-butyrate, (D_6)-propionate, (D_2)-valerate and (D_4)-hexanoate, (D_3)-lactate (CDN Isotopes, Quebec, Canada) were added. Samples were homogenized using a FastPrep-24 system (MP-Bio), with Matrix D at 60hz for 30 seconds, before being cleared of protein by centrifugation at 16,000xg. 60µL cleared supernatants were collected and derivatized using 3-nitrophenylhydrazine. Each sample was mixed with 20 µL of 200 mM 3-nitrophenylhydrazine in 50% aqueous acetonitrile and 20 µL of 120 mM N-(3-dimethylaminopropyl)-N0-ethylcarbodiimide -6% pyridine solution in 50% aqueous acetonitrile. The mixture was reacted at 50°C for 40 minutes and the reaction was stopped with 0.45 mL of 50% acetonitrile.

LC-MS Analysis

Derivatized samples were injected (50 µL) via a Thermo Vanquish UHPLC and separated over a reversed phase Phenomenex Kinetex 150mm x 2.1mm 1.7µM particle C18 maintained at 55°C. For the 20 minute LC gradient, the mobile phase consisted of the following: solvent A (water / 0.1% FA) and solvent B (ACN / 0.1% FA). The gradient was the following: 0-2min 15% B, increase to 60%B over 10 minutes, continue increasing to 100%B over 1 minute, hold at 100%B for 3 minutes, reequillibrate at 15%B for 4 minutes. The Thermo IDX tribrid mass spectrometer was operated in both positive ion mode, scanning in ddMS2 mode (2 µscans) from 75 to 1000 m/z at 120,000 resolution with an AGC target of 2e5 for full scan, 2e4 for ms2 scans using HCD fragmentation at stepped 15,35,50 collision energies. Source ionization setting was 3.0kV spray voltage respectively for positive mode. Source gas parameters were 45 sheath gas, 12 auxiliary gas at 320°C, and 3 sweep gas. Calibration was performed prior to analysis using the PierceTM FlexMix Ion Calibration Solutions (Thermo Fisher Scientific). Integrated peak areas were then extracted manually using Quan Browser (Thermo Fisher Xcalibur ver. 2.7). SCFA and TCA are reported as area ratio of SCFA or TCA to the internal standard(66).

Shallow Shotgun Sequencing

Stool pellets were collected from each mouse at day 0, 14, 28, and 38 of sucralose treatment. Each pellet was collected into a sterile microcentrifuge tube and stored at -80C prior to gDNA extraction with a Qiagen QIAamp Fast DNA Stool Mini Kit. After gDNA isolation, DNA was checked for concentration and purity before shipping to Microbiome Insights where paired-end sequencing (150 bp x 2) was done in a NovaSeq 6000 instrument.

Microbiome Taxonomic Analysis

Metagenomic sequencing data was processed using bioBakery KneadData (http://huttenhower.sph.harvard.edu/kneaddata, RRID:SCR_016596), which removed adapters and low-quality reads with Trimmomatic(67), repetitive sequences with TRF(68), as well as non-bacterial reads using Bowtie 2(69) by aligning against the human reference genome GRCh38 and the mouse reference genome GRCm39. MetaPhlAn 4(70) was run using the cleaned microbial reads to assign taxonomic

classifications with absolute abundances using the “-t rel_ab_w_read_stats” option. The native bioBakery SGB taxonomy assignments were converted to GTDB taxonomy(71) form using the sgb_to_gtdb.py script provided by the bioBakery developers. To maintain absolute abundance data, the taxonomy conversion script was modified as it only natively worked with relative abundance. MicrobiotaProcess(72) was used for downstream analysis and visualization of the absolute abundance data with GTDB taxonomy assignments. Specifically, MicrobiotaProcess was used to calculate alpha diversity, beta diversity, principal coordinate analysis of beta diversity, and cladogram plotting. Visualizations not created by MicrobiotaProcess were done using ggplot2(73). Groupwise comparisons for the species-level were made between each treatment group relative to the ctrl group at each timepoint using MaAsLin2(74).

Microbiome Functional Profiling

The cleaned microbial reads were functionally profiled using HUMAnN 3(75), which utilizes pangenomes detected by MetaPhlAn to annotate reads using UniRef90(76) gene family clusters. These UniRef90 gene family annotations are then further grouped into MetaCyc pathways(77). The output pathway abundance was normalized to copies per million (CPM) using the human_renorm_table script provided by the bioBakery developers. Normalized output was analyzed using MaAsLin2 within the microeco R package to utilize the full hierarchical pathway structure for MetaCyc(78). Groupwise comparisons were conducted across all timepoints and groups relative to day 0 and the ctrl group respectively. Significant pathways were plot using ggplot2.

Single cell and bulk RNA sequencing *ex vivo*

Sample Prep

C57Bl/6 mice sourced from Taconic were treated with sucralose 14 days prior to tumor injection with MC38. Mice were implanted with 250,000 MC38 cells on day 0 and treated with anti-PD-1 antibody on day 9 and 12 post implantation. Three mice from each of the sucralose+anti-PD-1 and anti-PD-1 groups were sacrificed on day 14. Tumor draining lymph nodes (right inguinal) and MC38 tumors were harvested and

processed into single cell suspensions. For bulk, single cell suspensions were stained and sorted on the Bigfoot Cell Sorter. CD8+ T cells and CD4+ T cells were sorted out separately (up to 1000 cells per sample) based on live+, CD90.2+, TCRb+, and CD4+ or CD8+. CD8+ T cells were further sorted out into CD44hi and CD44hi RPL18+. Cells were then placed into buffer in 96 well plate for storage for further analysis. For single cell, cell suspensions from tumor and lymph node were washed and labeled with 10x Genomics TotalSeq-C hashtags supplied by the University of Pittsburgh Sequencing Core as explained in the protocol provided by 10x Genomics.

Preprocessing data and clustering

We used CellRanger-7.0.0 to process the raw reads. Subsequent data processing, filtering, clustering and reduced dimensionality projections were all carried out using Seurat package version 4.4.0(79) in R 4.3.0. Both the dLN and tumor data were processed using the same pipeline. Processing of the data sets involved the filtering of cells with fewer than 100 genes expressed and cells with % of mitochondrial genes greater than 20%. Genes were also filtered based on the percentage of cells in which they were expressed. Finally, doublets and negatives, as identified by the Seurat function HTODemux, were taken out of the data set. Overall, for subsequent analyses, we used 34954 dLN cells and 41850 tumor cells.

To identify clusters in the data set, we a K-nearest neighbor (KNN) graph-based clustering as implemented in Seurat. Default parameters were applied throughout our analyses. All dimensionality reduction and projections were performed using Seurat, PCA (Principal Component Analysis) was run using default parameters, UMAP and tSNE were computed using the 10 first components of out of the PCA.

SLIDE analyses

We used SLIDE(33), an interpretable machine learning approach that relies on latent factor regression with strong statistical guarantees to infer transcriptomic differences across mice with and without exposure to sucralose. We built cell-specific SLIDE models for CD4+ T_{conv}, CD8+ T cells and Tregs from the dLN and CD4+ T_{conv}, CD8+ T cells from the tumor. Clusters were annotated with cell types using known marker genes

– CD4+ T_{conv} clusters were $CD4^+CD25^-CD62L^+CD44^-$, CD8+ T cells clusters were $CD3^+$, $CD5^+$, $CD8^+$, $CD27^+$, and CD28+, and Tregs clusters were $CD4^+CD25^+$. Overall, 5 models were built. Delta and spec were tuned using grid search, for other parameters default values were used.

SLIDE takes cell x gene matrices as inputs. The inputs to the 3 dLN models were 3308 cells x 3002 genes (CD8+ T cells), 12039 cells x 3032 genes matrix (for CD4+ T_{conv}) and 1242 cells x 3028 genes (Tregs). For the 2 tumor models,the inputs were 7276 cells x 3346 genes (CD8+ T cells) and 299 cells x 6079 genes (for CD4+ T_{conv}). Latent factor discovery and identification of significant latent factors were performed as described in SLIDE(33).

To rigorously evaluate the performance of the SLIDE models, we used a k-fold cross-validation framework with multiple replicates and permutation testing. Briefly, replicate k-fold cross-validation (k-fold CV) assesses the robustness of the model with data held out. It extends the basic k-fold cross-validation method by conducting the entire k-fold process multiple times, with each iteration (replication) involving a new random partitioning of the dataset into *k* distinct folds. In each of these folds, k-1 folds are used for training the model, and 1-fold for testing it, ensuring that every data point is in the test fold exactly once (for each replicate). This process helps assess model performance on data held out (an overfit model would only do well on training but not test data). Additionally, model significance is assessed using permutation testing. This involves shuffling the labels of the dataset in a matched cross-validation framework. By comparing actual model performance against this empirical null derived from models built using shuffled labels, we assess the significance of the models (exact P values calculated using permutating testing). We used 10 replicates of 10-fold CV for the dLN models, and 20 replicates of 10-fold CV for the tumor models.

Bulk RNA Sequencing from in vitro cell cultures

RNA was isolated from day 7 in vitro cell cultures using Qiagen RNeasy Mini Kits. After RNA isolation, libraries were prepared using the Illumina stranded mRNA Preps. Sequencing was performed using an Illumina NextSeq 2000 Sequencing System. After sequencing, reads were aligned to the mm10 genome assembly using STAR alignment.

Reads were quantified to an annotation model with Partek Flow using Partek E/M quantitation. Counts were then normalized by median ratio, and differential expression analysis was performed using DESeq2.

Statistics

Statistical analyses were performed in GraphPad Prism v10. Data are presented as the mean +/- SEM. Statistical significance was determined using student's T test when comparing two groups, one-way ANOVA when comparing more than two groups, or a two-way ANOVA when comparing more than two groups over time. For more detail on significance, please see figure legends.

Data availability

The datasets generated are available at GEO: bulk RNAseq on $CD8^+$ T cells after activation and expansion in sucralose and single cell RNAseq on $CD45^+$ cells isolated from tumor and tumor draining lymph node of mice consuming sucralose-containing water or regular water (GSE260936). Codebase is available on GitHub (https://github.com/jishnu-lab/SucralosePD1). Shallow shotgun data were deposited at SRA (PRJNA1090098).

Acknowledgments: The authors would like to thank M. Meyer from the UPMC Hillman Cancer Center Flow Core for cell sorting; H. Monroe, R. Lafyatis, and the UPMC Genome Center for preparation and sequencing of scRNA-seq samples; the staff of the Division of Laboratory Animal Services for the animal husbandry; the Health Sciences Mass Spectrometry Core, the Pitt Biospecimen Core-Research Histology, the UPMC Hillman Cancer Center Flow Core, the Center for Research Computing, the Tumor Microenvironment Center, the Department of Immunology as well as members of the Delgoffe, Das, Davar, and Overacre Labs for helpful discussions. Research reported in this publication was supported by the National Cancer Institute of the National Institutes of Health under Award Number P30CA047904. Funding that supported this work includes: National Institutes of Health grant DP2AI177967 (AEO-D), Damon Runyon Cancer Research Foundation (AEO-D), National Institutes of Health grant S10OD023402 (SLG), National Institutes of Health grant S10OD032141 (SLG), National

Institutes of Health grant R01CA206517 (LPK), National Institutes of Health grant R01AI138504 (LPK), National Institutes of Health grant T32GM008208 (HNR) National Institutes of Health grant U01 CA271407, R01 CA257265, U01 CA268806, and P50 CA254865 (D.D.), Gateway Foundation for Cancer Research grant G-22-800 (SLG)

960

Author contributions:

A.E.O-D and K.M. participated in the conceptualization of the study. K.M., D.W., B.X., Z.D., M.N., S.J.M. performed and analyzed all experiments with support and supervision from S.L.G., J.D., D.D., G.M.D., and A.E.O-D. Dietary data was collected and analyzed by MN and DH with support and supervision from DD, and AEO-D. Statistical analyses for human cancer patients were performed by HW. Microbiome analysis was performed by M.M. with supervision from D.R.. Project administration was performed by D.D., J.D., L.K., G.M.D., and A.E.O-D. The original draft was written by K.M., D.W., D.D. and AEO-D. All authors reviewed and edited the manuscript.

965

970

975

980

985

References

1. Aggarwal V, Workman CJ, Vignali DAA. LAG-3 as the third checkpoint inhibitor. Nat Immunol. 2023;24:1415–22.

2. Olivares-Hernández A, González Del Portillo E, Tamayo-Velasco Á, Figuero-Pérez L, Zhilina-Zhilina S, Fonseca-Sánchez E, et al. Immune checkpoint inhibitors in non-small cell lung cancer: from current perspectives to future treatments-a systematic review. Ann Transl Med. 2023;11:354.

3. Tumeh PC, Harview CL, Yearley JH, Shintaku IP, Taylor EJM, Robert L, et al. PD-1 blockade induces responses by inhibiting adaptive immune resistance. Nature. 2014;515:568–71.

4. Fortman D, Karunamurthy A, Hartman D, Wang H, Seigh L, Abukhiran I, et al. Automated Quantitative CD8+ Tumor-Infiltrating Lymphocytes and Tumor Mutation Burden as Independent Biomarkers in Melanoma Patients Receiving Front-Line Anti-PD-1 Immunotherapy. Oncologist. 2024;29:619–28.

5. Herbst RS, Soria J-C, Kowanetz M, Fine GD, Hamid O, Gordon MS, et al. Predictive correlates of response to the anti-PD-L1 antibody MPDL3280A in cancer patients. Nature. 2014;515:563–7.

6. Taube JM, Klein A, Brahmer JR, Xu H, Pan X, Kim JH, et al. Association of PD-1, PD-1 ligands, and other features of the tumor immune microenvironment with response to anti-PD-1 therapy. Clin Cancer Res. 2014;20:5064–74.

7. Rizvi H, Sanchez-Vega F, La K, Chatila W, Jonsson P, Halpenny D, et al. Molecular Determinants of Response to Anti-Programmed Cell Death (PD)-1 and Anti-Programmed Death-Ligand 1 (PD-L1) Blockade in Patients With Non-Small-Cell Lung Cancer Profiled With Targeted Next-Generation Sequencing. J Clin Oncol. 2018;36:633–41.

8. Rizvi NA, Hellmann MD, Snyder A, Kvistborg P, Makarov V, Havel JJ, et al. Cancer immunology. Mutational landscape determines sensitivity to PD-1 blockade in non-small cell lung cancer. Science. 2015;348:124–8.

9. Chowell D, Morris LGT, Grigg CM, Weber JK, Samstein RM, Makarov V, et al. Patient HLA class I genotype influences cancer response to checkpoint blockade immunotherapy. Science. 2018;359:582–7.

10. Matson V, Fessler J, Bao R, Chongsuwat T, Zha Y, Alegre M-L, et al. The commensal microbiome is associated with anti-PD-1 efficacy in metastatic melanoma patients. Science. 2018;359:104–8.

11. Fidelle M, Rauber C, Alves Costa Silva C, Tian A-L, Lahmar I, de La Varende A-LM, et al. A microbiota-modulated checkpoint directs immunosuppressive intestinal T cells into cancers. Science. 2023;380:eabo2296.

12. Spencer CN, McQuade JL, Gopalakrishnan V, McCulloch JA, Vetizou M, Cogdill AP, et al. Dietary fiber and probiotics influence the gut microbiome and melanoma immunotherapy response. Science. 2021;374:1632–40.

13. Gopalakrishnan V, Spencer CN, Nezi L, Reuben A, Andrews MC, Karpinets TV, et al. Gut microbiome modulates response to anti-PD-1 immunotherapy in melanoma patients. Science. 2018;359:97–103.

14. Routy B, Le Chatelier E, Derosa L, Duong CPM, Alou MT, Daillère R, et al. Gut microbiome influences efficacy of PD-1-based immunotherapy against epithelial tumors. Science. 2018;359:91–7.

15. Belkaid Y, Hand TW. Role of the microbiota in immunity and inflammation. Cell. 2014;157:121–41.

16. Singh RK, Chang H-W, Yan D, Lee KM, Ucmak D, Wong K, et al. Influence of diet on the gut microbiome and implications for human health. J Transl Med. 2017;15:73.

17. Bäckhed F, Ley RE, Sonnenburg JL, Peterson DA, Gordon JI. Host-bacterial mutualism in the human intestine. Science. 2005;307:1915–20.

18. David LA, Maurice CF, Carmody RN, Gootenberg DB, Button JE, Wolfe BE, et al. Diet rapidly and reproducibly alters the human gut microbiome. Nature. 2014;505:559–63.

19. Arumugam M, Raes J, Pelletier E, Le Paslier D, Yamada T, Mende DR, et al. Enterotypes of the human gut microbiome. Nature. 2011;473:174–80.

20. Sonnenburg ED, Smits SA, Tikhonov M, Higginbottom SK, Wingreen NS, Sonnenburg JL. Diet-induced extinctions in the gut microbiota compound over generations. Nature. 2016;529:212–5.

21. Smits SA, Leach J, Sonnenburg ED, Gonzalez CG, Lichtman JS, Reid G, et al. Seasonal cycling in the gut microbiome of the Hadza hunter-gatherers of Tanzania. Science. 2017;357:802–6.

22. Vangay P, Johnson AJ, Ward TL, Al-Ghalith GA, Shields-Cutler RR, Hillmann BM, et al. US immigration westernizes the human gut microbiome. Cell. 2018;175:962-972.e10.

23. Sørensen TIA, Martinez AR, Jørgensen TSH. Epidemiology of Obesity. Handb Exp Pharmacol. 2022;274:3–27.

24. Suez J, Korem T, Zeevi D, Zilberman-Schapira G, Thaiss CA, Maza O, et al. Artificial sweeteners induce glucose intolerance by altering the gut microbiota. Nature. 2014;514:181–6.

25. Suez J, Cohen Y, Valdés-Mas R, Mor U, Dori-Bachash M, Federici S, et al. Personalized microbiome-driven effects of non-nutritive sweeteners on human glucose tolerance. Cell. 2022;185:3307-3328.e19.

26. Méndez-García LA, Bueno-Hernández N, Cid-Soto MA, De León KL, Mendoza-Martínez VM, Espinosa-Flores AJ, et al. Ten-Week Sucralose Consumption Induces Gut Dysbiosis and Altered Glucose and Insulin Levels in Healthy Young Adults. Microorganisms. 2022;10(2):434.

27. Zani F, Blagih J, Gruber T, Buck MD, Jones N, Hennequart M, et al. The dietary sweetener sucralose is a negative modulator of T cell-mediated responses. Nature. 2023;615:705–11.

28. Davar D, Morrison RM, Dzutsev AK, Karunamurthy A, Chauvin J-M, Amatore F, et al. Neoadjuvant vidutolimod and nivolumab in high-risk resectable melanoma: A prospective phase II trial. Cancer Cell. 2024;42:1898-1918.e12.

29. Thiele C, Hirschfeld G. cutpointr : improved estimation and validation of optimal cutpoints in *r*. J Stat Softw. 2021;98(11):1-27.

30. Nair AB, Jacob S. A simple practice guide for dose conversion between animals and human. J Basic Clin Pharm. 2016;7:27–31.

31. Caruso R, Ono M, Bunker ME, Núñez G, Inohara N. Dynamic and Asymmetric Changes of the Microbial Communities after Cohousing in Laboratory Mice. Cell Rep. 2019;27:3401-3412.e3.

32. Harley ITW, Giles DA, Pfluger PT, Burgess SL, Walters S, Hembree J, et al. Differential colonization with segmented filamentous bacteria and Lactobacillus murinus do not drive divergent development of diet-induced obesity in C57BL/6 mice. Mol Metab. 2013;2:171–83.

33. Rahimikollu J, Xiao H, Rosengart A, Rosen ABI, Tabib T, Zdinak PM, et al. SLIDE: Significant Latent Factor Interaction Discovery and Exploration across biological domains. Nat Methods. 2024;21:835–45.

34. Akamatsu M, Mikami N, Ohkura N, Kawakami R, Kitagawa Y, Sugimoto A, et al. Conversion of antigen-specific effector/memory T cells into Foxp3-expressing Treg cells by inhibition of CDK8/19. Sci Immunol. 2019;4(40):eaaw2707.

35. Li H, van der Leun AM, Yofe I, Lubling Y, Gelbard-Solodkin D, van Akkooi ACJ, et al. Dysfunctional CD8 T Cells Form a Proliferative, Dynamically Regulated Compartment within Human Melanoma. Cell. 2019;176:775-789.e18.

36. Scotto di Carlo F, Russo S, Muyas F, Mangini M, Garribba L, Pazzaglia L, et al. Profilin 1 deficiency drives mitotic defects and reduces genome stability. Commun Biol. 2023;6:9.

37. Wherry EJ, Kurachi M. Molecular and cellular insights into T cell exhaustion. Nat Rev Immunol. 2015;15:486–99.

38. Rochman Y, Spolski R, Leonard WJ. New insights into the regulation of T cells by gamma(c) family cytokines. Nat Rev Immunol. 2009;9:480–90.

39. Chinen T, Kannan AK, Levine AG, Fan X, Klein U, Zheng Y, et al. An essential role for the IL-2 receptor in Treg cell function. Nat Immunol. 2016;17:1322–33.

40. Friedline RH, Brown DS, Nguyen H, Kornfeld H, Lee J, Zhang Y, et al. CD4+ regulatory T cells require CTLA-4 for the maintenance of systemic tolerance. J Exp Med. 2009;206:421–34.

41. Tai X, Van Laethem F, Pobezinsky L, Guinter T, Sharrow SO, Adams A, et al. Basis of CTLA-4 function in regulatory and conventional CD4(+) T cells. Blood. 2012;119:5155–63.

42. Wing K, Onishi Y, Prieto-Martin P, Yamaguchi T, Miyara M, Fehervari Z, et al. CTLA-4 control over Foxp3+ regulatory T cell function. Science. 2008;322:271–5.

43. Tenger C, Zhou X. Apolipoprotein E modulates immune activation by acting on the antigen-presenting cell. Immunology. 2003;109:392–7.

44. Myers LM, Tal MC, Torrez Dulgeroff LB, Carmody AB, Messer RJ, Gulati G, et al. A functional subset of CD8+ T cells during chronic exhaustion is defined by SIRPα expression. Nat Commun. 2019;10:794.

45. Morzadec C, Macoch M, Sparfel L, Kerdine-Römer S, Fardel O, Vernhet L. Nrf2 expression and activity in human T lymphocytes: stimulation by T cell receptor activation and priming by inorganic arsenic and tert-butylhydroquinone. Free Radic Biol Med. 2014;71:133–45.

46. Sivan A, Corrales L, Hubert N, Williams JB, Aquino-Michaels K, Earley ZM, et al. Commensal Bifidobacterium promotes antitumor immunity and facilitates anti-PD-L1 efficacy. Science. 2015;350:1084–9.

47. Vétizou M, Pitt JM, Daillère R, Lepage P, Waldschmitt N, Flament C, et al. Anticancer immunotherapy by CTLA-4 blockade relies on the gut microbiota. Science. 2015;350:1079–84.

48. Lee KA, Thomas AM, Bolte LA, Björk JR, de Ruijter LK, Armanini F, et al. Cross-cohort gut microbiome associations with immune checkpoint inhibitor response in advanced melanoma. Nat Med. 2022;28:535–44.

49. McCulloch JA, Davar D, Rodrigues RR, Badger JH, Fang JR, Cole AM, et al. Intestinal microbiota signatures of clinical response and immune-related adverse events in melanoma patients treated with anti-PD-1. Nat Med. 2022;28:545–56.

50. Smith M, Dai A, Ghilardi G, Amelsberg KV, Devlin SM, Pajarillo R, et al. Gut microbiome correlates of response and toxicity following anti-CD19 CAR T cell therapy. Nat Med. 2022;28:713–23.

51. Davar D, Dzutsev AK, McCulloch JA, Rodrigues RR, Chauvin J-M, Morrison RM, et al. Fecal microbiota transplant overcomes resistance to anti-PD-1 therapy in melanoma patients. Science. 2021;371:595–602.

52. Routy B, Lenehan JG, Miller WH, Jamal R, Messaoudene M, Daisley BA, et al. Fecal microbiota transplantation plus anti-PD-1 immunotherapy in advanced melanoma: a phase I trial. Nat Med. 2023;29:2121–32.

53. Geiger R, Rieckmann JC, Wolf T, Basso C, Feng Y, Fuhrer T, et al. L-Arginine Modulates T Cell Metabolism and Enhances Survival and Anti-tumor Activity. Cell. 2016;167:829-842.e13.

54. Kim YJ, Lee J-Y, Lee JJ, Jeon SM, Silwal P, Kim IS, et al. Arginine-mediated gut microbiome remodeling promotes host pulmonary immune defense against nontuberculous mycobacterial infection. Gut Microbes. 2022;14:2073132.

55. Agarwal U, Didelija IC, Yuan Y, Wang X, Marini JC. Supplemental citrulline is more efficient than arginine in increasing systemic arginine availability in mice. J Nutr. 2017;147:596–602.

56. Riquelme E, Zhang Y, Zhang L, Montiel M, Zoltan M, Dong W, et al. Tumor microbiome diversity and composition influence pancreatic cancer outcomes. Cell. 2019;178:795-806.e12.

57. Wastyk HC, Fragiadakis GK, Perelman D, Dahan D, Merrill BD, Yu FB, et al. Gut-microbiota-targeted diets modulate human immune status. Cell. 2021;184:4137-4153.e14.

58. Jiang Y, Farias R, Holly AE, Levy EJ, Klein L, Rains J, et al. The DIET study: A randomized controlled trial of a high fiber diet intervention (HFDI) in patients (pts) with melanoma receiving immune checkpoint blockade (ICB). JCO. 2024;42:9558–9558.

59. Turnbaugh PJ, Ridaura VK, Faith JJ, Rey FE, Knight R, Gordon JI. The effect of diet on the human gut microbiome: a metagenomic analysis in humanized gnotobiotic mice. Sci Transl Med. 2009;1:6ra14.

60. Eisenhauer EA, Therasse P, Bogaerts J, Schwartz LH, Sargent D, Ford R, et al. New response evaluation criteria in solid tumours: revised RECIST guideline (version 1.1). Eur J Cancer. 2009;45:228–47.

61. Cottrell TR, Thompson ED, Forde PM, Stein JE, Duffield AS, Anagnostou V, et al. Pathologic features of response to neoadjuvant anti-PD-1 in resected non-small-cell lung carcinoma: a proposal for quantitative immune-related pathologic response criteria (irPRC). Ann Oncol. 2018;29:1853–60.

62. Stein JE, Soni A, Danilova L, Cottrell TR, Gajewski TF, Hodi FS, et al. Major pathologic response on biopsy (MPRbx) in patients with advanced melanoma treated with anti-PD-1: evidence for an early, on-therapy biomarker of response. Ann Oncol. 2019;30:589–96.

63. Tetzlaff MT, Messina JL, Stein JE, Xu X, Amaria RN, Blank CU, et al. Pathological assessment of resection specimens after neoadjuvant therapy for metastatic melanoma. Ann Oncol. 2018;29:1861–8.

64. History of the Diet History Questionnaire (DHQ) | EGRP/DCCPS/NCI/NIH [Internet]. [cited 2024 Nov 20]. Available from: https://epi.grants.cancer.gov/dhq3/

65. Millen AE, Midthune D, Thompson FE, Kipnis V, Subar AF. The National Cancer Institute diet history questionnaire: validation of pyramid food servings. Am J Epidemiol. 2006;163:279–88.

66. Han J, Lin K, Sequeira C, Borchers CH. An isotope-labeled chemical derivatization method for the quantitation of short-chain fatty acids in human feces by liquid chromatography-tandem mass spectrometry. Anal Chim Acta. 2015;854:86–94.

67. Bolger AM, Lohse M, Usadel B. Trimmomatic: A flexible trimmer for Illumina sequence data. Bioinformatics. 2014;30:2114–20.

68. Benson G. Tandem repeats finder: a program to analyze DNA sequences. Nucleic Acids Res. 1999;27:573–80.

69. Langmead B, Salzberg SL. Fast gapped-read alignment with Bowtie 2. Nat Methods. 2012;9:357–9.

70. Blanco-Míguez A, Beghini F, Cumbo F, McIver LJ, Thompson KN, Zolfo M, et al. Extending and improving metagenomic taxonomic profiling with uncharacterized species using MetaPhlAn 4. Nat Biotechnol. 2023;41:1633–44.

71. Parks DH, Chuvochina M, Rinke C, Mussig AJ, Chaumeil P-A, Hugenholtz P. GTDB: an ongoing census of bacterial and archaeal diversity through a phylogenetically consistent, rank normalized and complete genome-based taxonomy. Nucleic Acids Res. 2022;50:D785–94.

72. Xu S, Zhan L, Tang W, Wang Q, Dai Z, Zhou L, et al. MicrobiotaProcess: A comprehensive R package for deep mining microbiome. Innovation (Camb). 2023;4:100388.

73. ggplot2: Elegant Graphics for Data Analysis | SpringerLink [Internet]. [cited 2024 Nov 20]. Available from: https://link.springer.com/book/10.1007/978-3-319-24277-4

74. Mallick H, Rahnavard A, McIver LJ, Ma S, Zhang Y, Nguyen LH, et al. Multivariable association discovery in population-scale meta-omics studies. PLoS Comput Biol. 2021;17:e1009442.

75. Beghini F, McIver LJ, Blanco-Míguez A, Dubois L, Asnicar F, Maharjan S, et al. Integrating taxonomic, functional, and strain-level profiling of diverse microbial communities with bioBakery 3. eLife. 2021;10.

76. Suzek BE, Wang Y, Huang H, McGarvey PB, Wu CH, UniProt Consortium. UniRef clusters: a comprehensive and scalable alternative for improving sequence similarity searches. Bioinformatics. 2015;31:926–32.

77. Caspi R, Billington R, Keseler IM, Kothari A, Krummenacker M, Midford PE, et al. The MetaCyc database of metabolic pathways and enzymes - a 2019 update. Nucleic Acids Res. 2020;48:D445–53.

78. Liu C, Cui Y, Li X, Yao M. microeco: an R package for data mining in microbial community ecology. FEMS Microbiol Ecol. 2021;97.

79. Hao Y, Hao S, Andersen-Nissen E, Mauck WM, Zheng S, Butler A, et al. Integrated analysis of multimodal single-cell data. Cell. 2021;184:3573-3587.

Figure Legends:

Figure 1. Non-nutritive sweetener (NNS) intake is associated with poor response to immune checkpoint blockade (ICI) in advanced melanoma, advanced NSCLC and neoadjuvant melanoma. a, Advanced melanoma, advanced NSCLC and neoadjuvant melanoma patients pending receipt of ICI therapy completed web-based semiquantitative FFQ DHQ III. Response to therapy was evaluated using investigator-assessed objective radiographic rate (ORR) using RECIST v1.1 or pathologist-assessed immune-related pathologic response criteria, along with time-to-event analyses including PFS (advanced melanoma or NSCLC) or RFS (neoadjuvant melanoma). RFS/PFS were evaluated every 3 months, and relapse/progression was defined based on radiographic and/or clinical relapse/progression at each treatment visit (every 3–4 weeks). **a**, Patients were dichotomized into high- and low- intake groups based on cutpointr-determined endpoints. **b and c**, Proportion of investigator-assessed ORR in either melanoma (**b**) or NSCLC (**c**) cohorts. Chi-squared p values comparing responder ORR between high vs. low intake are shown. **d and e**, Kaplan-Meier plots of PFS probability of ICI-treated melanoma (**d**) and NSCLC (**e**) patients based on dichotomized sucralose intake levels by two-sided log-rank test are shown. Number of people at risk in in either group (high vs. low intake) is shown below each panel. Vertical ticks show censored data. **f**, Proportion of pathologist-assessed major pathologic response (MPR, defined as 0-10% residual viable tumor) between high and low sucralose intake in patients with high-risk resectable melanoma treated with nivolumab and TLR9 agonist vidutolimod. Chi-squared p-values comparing responder MPR between high and low intake are shown. **g**, Kaplan-Meier plots of RFS probability of patients with neoadjuvant nivolumab/vidutolimod treated melanoma based on dichotomized sucralose intake levels by two-sided log-rank test are shown. Number of people at risk in in either group (high vs. low intake) is shown below each panel. Vertical ticks show censored data.

Figure 2. Sucralose ablates immunotherapeutic response. C57Bl/6 mice from Taconic consumed sucralose in the drinking water (0.09mg/mL) for 2 weeks prior to tumor injection and for the duration of the experiment. Mice were injected with $2.5x10^5$ MC38 cells subcutaneously and treated with 200µg anti-PD1 on days 9, 12, and 15. Tumor area was measured every 3 days until endpoint. **a,** Experimental schematic. **b,** Tumor growth curves of mice consuming sucrose or sucralose in the drinking water during treatment with anti-PD1. **c,** Tumor growth curves in MC38 s.c. (circles) or B16 i.d. (squares) treated with anti-PD1. Mice were sourced from either Jackson Labs (Jax, open circles) or Taconic (Tac, closed circles). Mice were removed from study either when tumors reached 2cm in either direction or if there was unresolved ulceration. Mean tumor growth lines halt once all mice in a treatment group were removed. **d-e,** C57Bl/6 mice from either Taconic (**d**) or Jackson (**e**) consumed sucralose in their drinking water as in (**c**). They were subjected to the AOM-DSS protocol (injected with 10mg/kg Azoxymethane (AOM) on D0 and given 3% DSS in the drinking water on D7-14 and 28-35). Overall tumor number and composition of ‘large’ tumors (>2mm in any

direction) are shown. Data are a composite of 3 (**c**) or 2 (**b,d**) independent experiments with 5 mice per group per experiment. Error bars represent the mean ± SEM. two-way ANOVA (**c**) or student's T test (**d**) were used. *p<0.05.

Figure 3. Sucralose alters the tumor microenvironment and supports T cell dysfunction. C57Bl/6 mice from Taconic consumed sucralose in the drinking water (0.09mg/mL) for 2 weeks prior to tumor injection and for the duration of the experiment. Mice were injected with $2.5x10^5$ MC38 cells subcutaneously and treated with 200µg anti-PD1 on days 9, and 12. **a-d,** $CD45^+$ cells were isolated from the tumor and tumor draining lymph node (dLN) prior to single cell RNA sequencing on day 14 post tumor injection. **a-b,** UMAP of clusters identified in dLN (**a**) and tumor (**b**) in mice treated with anti-PD1 +/- sucralose. **c,** Volcano plot of gene expression from $CD8^+$ T cells in the tumor of Sucralose+anti-PD1 vs anti-PD1 treated mice. **d,** Exhaustion signature heatmap for $CD8^+$ T cells in the tumor comparing Sucralose+anti-PD1 (purple) to anti-PD1 (teal). **e**, Representative flow plots and quantification of Mitotracker DeepRed staining in $CD8^+$ T cells or $CD4^+$ T conventional cells from draining (dLN). **f,** Representative flow plots of TNFα and IFNγ staining in $CD8^+$ T cells and $CD4^+$ T conventional cells in the tumor tissue of mice consuming sucralose and/or anti-PD1. Responder mice in anti-PD1+/-sucralose groups are shown as diamonds. Data are representative (**e**) or a composite (**f**) of 3 or 1 (**a-e**) independent experiments, respectively, with 5 mice per group per experiment. Error bars represent the mean ± SEM. One-way ANOVA with Tukey's multiple comparisons test (**e-f**) was used. *p<0.05, **p<0.005.

Figure 4. The gut microbiota is necessary and sufficient to drive immunotherapy resistance due to sucralose. a, Mice consumed sucralose (0.09mg/mL) in the drinking water for 14 days prior to antibiotic treatment and for the duration of the experiment. After 21 days of sucralose supplementation with or without antibiotics, mice were injected with $2.5x10^5$ MC38 cells subcutaneously and treated with anti-PD1 on days 9, 12, and 15. **b,** Tumor growth curve and overall survival plot of experiment described in (**a**). **c,** Fecal microbiome transfer (FMT) experimental overview. Donor mice (red) were given sucralose-supplemented drinking water (0.09mg/mL) for 2 weeks prior to donating stool. Stool was transferred to sucralose naïve recipient mice (light pink) that had received broad spectrum antibiotics for 7 days prior to transfer. Tumors were injected as previously described in 4a and measured until endpoint. **d,** Tumor growth curve of the experiment described in (**c**). Data are a composite of 3 (**b-c**) independent experiments with 5 mice per group per experiment. Error bars represent the mean ± SEM. Two-way ANOVA (**b,d**) was used. *p<0.05.

Figure 5. Responder-derived FMT is sufficient to restore immunotherapeutic response. a, Individual tumor growth curves from Fig. 4d with FMT. **b-c,** C57Bl/6 mice from Taconic consumed sucralose in the drinking water (0.09mg/mL) for 2 weeks prior to tumor injection and for the duration of the experiment. Mice were injected with $2.5x10^5$ MC38 cells subcutaneously and treated with 200µg anti-PD1 on days 9, 12, and 15. Tumor area was measured every 3 days until endpoint. 4 groups all received an

FMT from an anti-PD1 responder mouse donor. The following 4 groups were used: antibiotic treatment pre-FMT, continued sucralose consumption (hot pink), antibiotic treatment pre-FMT, stopped sucralose consumption (light pink), no antibiotics, continued sucralose consumption (purple), no antibiotics, stopped sucralose consumption (light blue). Individual tumor growth curves (**b**) and a composite growth curve and overall survival (**c**) are shown. Data are a composite of 3 (**a**) or 2 (**b-c**) independent experiments with 5 mice per group per replicate. Error bars represent the mean ± SEM. For growth curve statistics, 2-way ANOVA was used. Overall survival statistics were calculated using a log-rank Mantel-Cox test. *p<0.05.

Figure 6. Sucralose consumption shifts gut microbiome diversity and function. C57Bl/6 mice from Taconic consumed sucralose in the drinking water (0.09mg/mL) for 2 weeks prior to tumor injection and for the duration of the experiment. Mice were injected with $2.5x10^5$ MC38 cells subcutaneously and treated with 200µg anti-PD1 on days 9, 12, and 15. **a,** PCoA plot of the gut microbiome of sucralose-consuming versus abstaining mice on day 38. Serial stool collections were obtained on days 0,14,28, and 38 after start of sucralose consumption and sent for shallow shotgun sequencing. **b,** Cladogram with significantly overexpressed taxa in anti-PD1 or sucralose + anti-PD1 groups at day 38. **c,** Taxonomic relative abundance bar plots for the groups at day 38. % Abundance on the y-axis indicates the mean abundance for all mice within each group. Asterisks label bacterial species that are arginine degrading and enriched in sucralose-consuming groups. **d,** Functional pathway analysis of sucralose+anti-PD1 vs anti-PD1. Bar chart shows significant pathways with the default MaAsLin2 fdr threshold of <0.25. The MaAsLin2 coef value is reported on the x axis. **e,** Functional pathway analysis of the arginine degradation pathway between sucralose + anti-PD1 and anti-PD1. Heatmap shows fold change of arginine-degrading enzymes expressed by bacteria in sucralose-consuming groups. Data are representative of 1 independent experiment with 5 mice per group.

Figure 7. Citrulline supplementation restores T cell function and immunotherapy efficacy. a-c, Serum and tumor interstitial fluid was isolated from mice consuming sucralose-supplemented (0.09mg/mL) drinking water or regular drinking water for 14 days prior to tumor injection and throughout tumor growth. High-resolution LC-HRMS metabolomics analysis was performed **a,** Pathway analysis of tumor interstitial fluid, significant pathways are shown. **b,** Volcano plot comparing metabolite abundance from the tumor interstitial fluid of mice consuming sucralose in the drinking water versus regular water. **c,** Quantification of arginine abundance within the serum and tumor interstitial fluid of mice indicated. **d,** Taconic mice were given sucralose-supplemented (0.09mg/mL) or control drinking water in the presence of absence of arginine or citrulline (3.75mg/mL) for 2 weeks prior to tumor injection and throughout the duration of the experiment. Mice were injected with $2.5x10^5$ MC38 cells subcutaneously and treated with 200µg anti-PD1 at days 9, 12, and 15. **e,** Quantification of $IFN\gamma^+$ $CD8^+$ T cells and $CD4^+$ T conventional cells within the tumor 14 days after tumor injection. **f-g,** Tumor growth curves of mice from experiment described in (**d**). **g,** Tumor growth curves from experiment described in (d). Data are a composite of 3 (**e-h**), 2 (**c**) or 1 (**a-b**)

independent experiments with 3-5 mice per group per experiment. Error bars represent the mean ± SEM. Student's t-test (**c**), one-way ANOVA with Tukey's multiple comparisons test **(e),** Two-way ANOVA (**f-g**), and Mantel-Cox **(h)** was used. *p<0.05, **p<0.005, ****p<0.00005

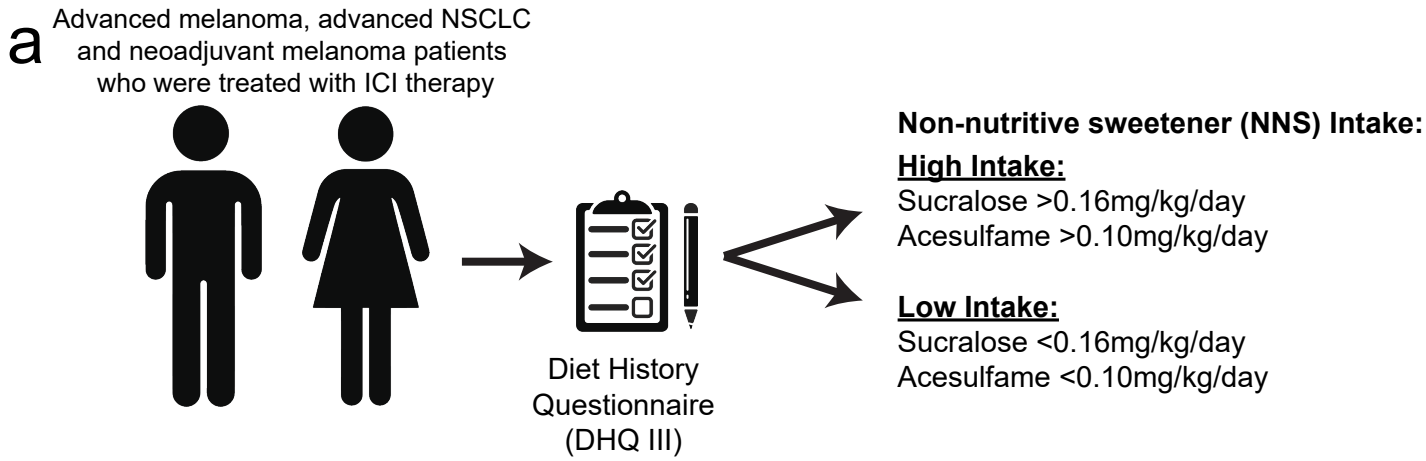

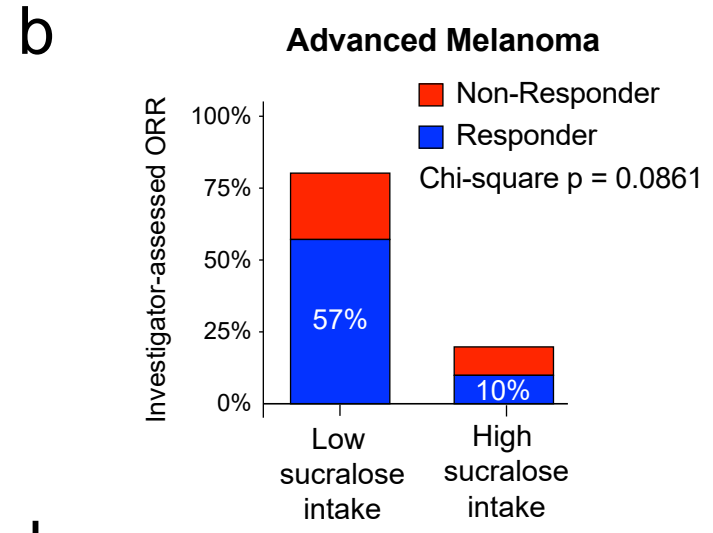

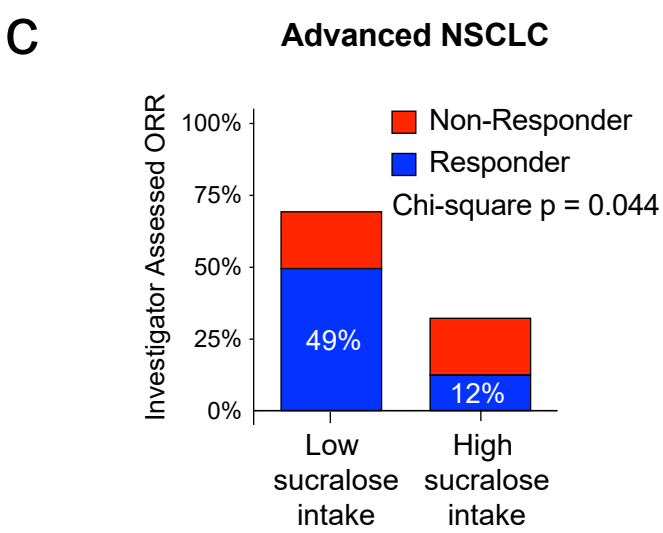

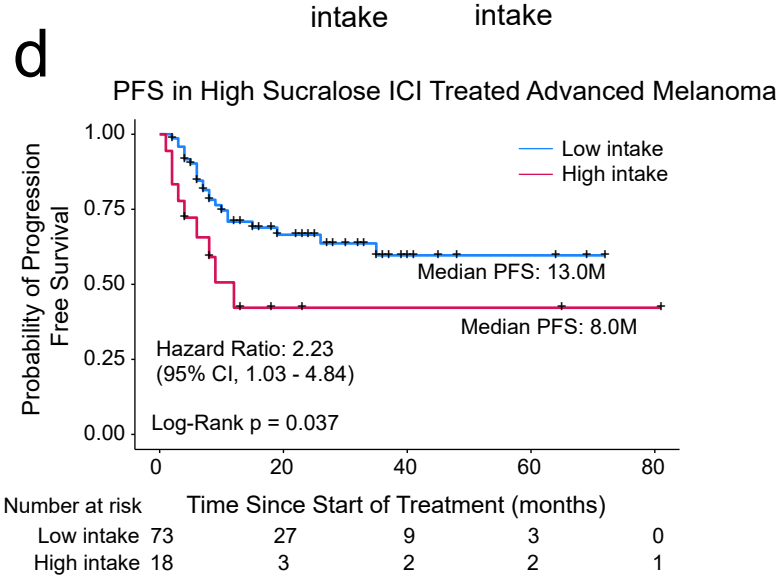

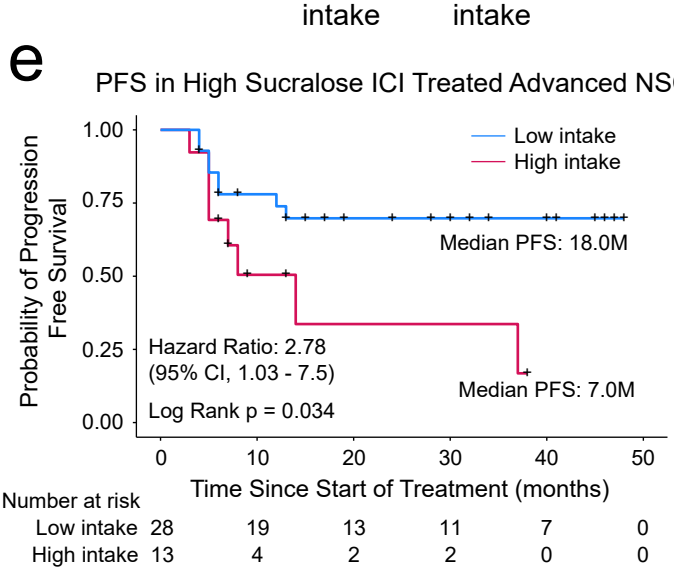

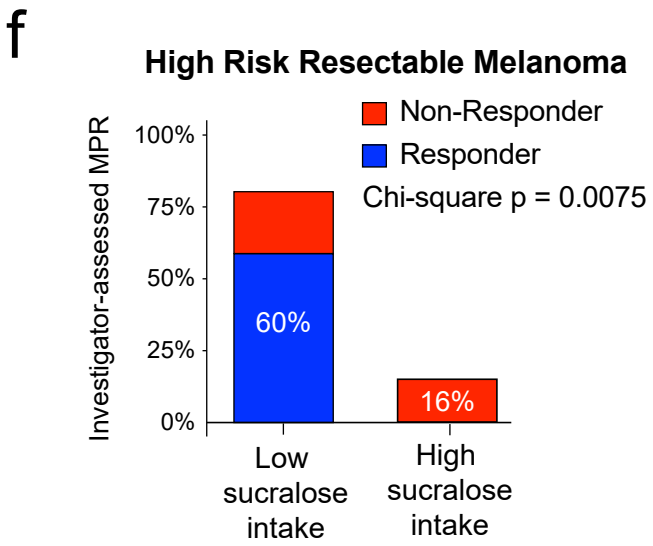

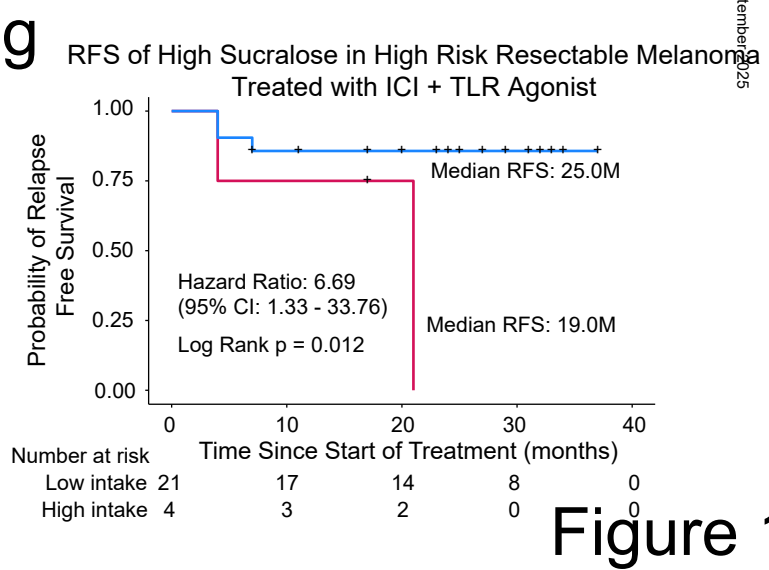

Figure 1

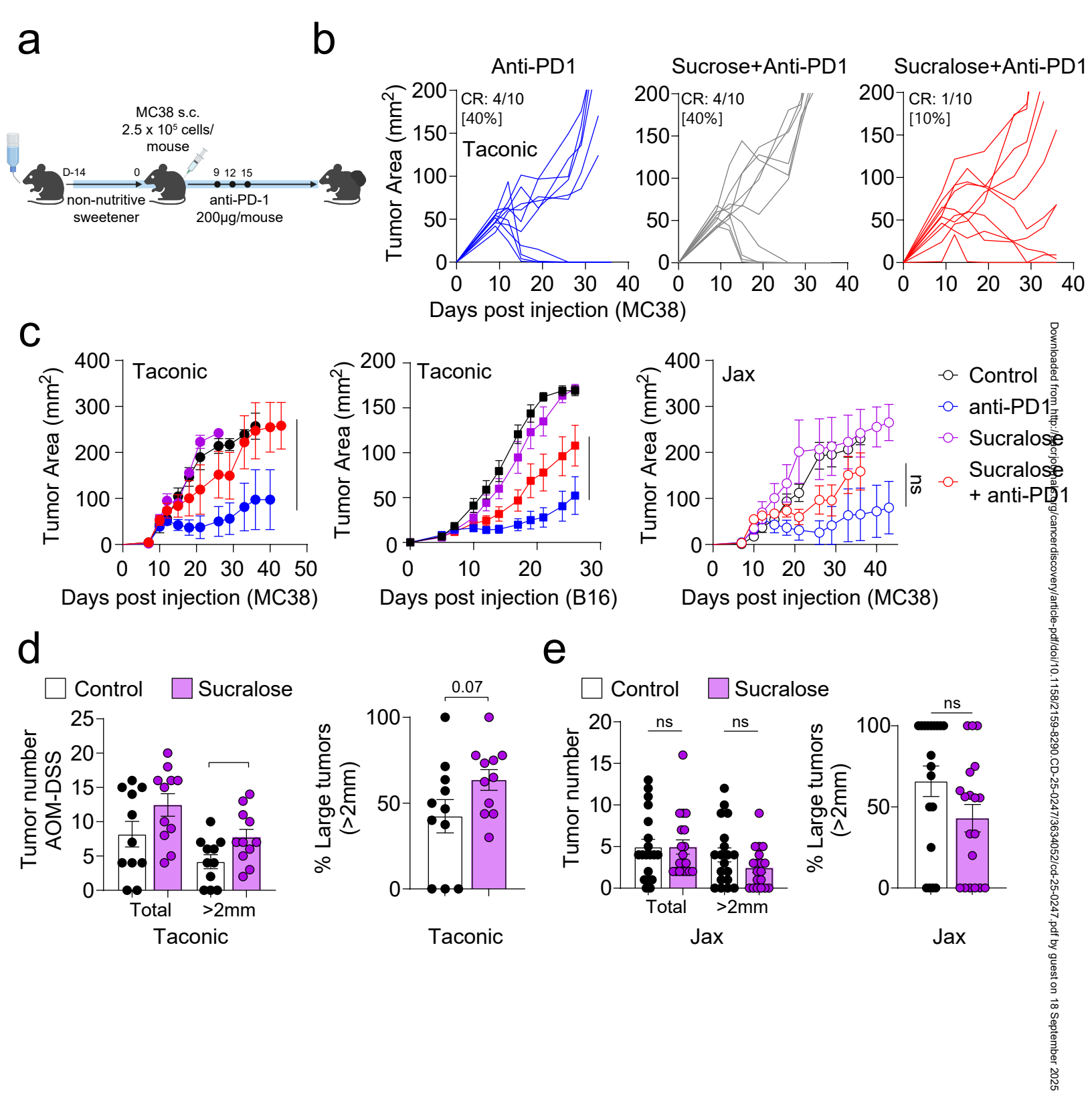

Figure 2

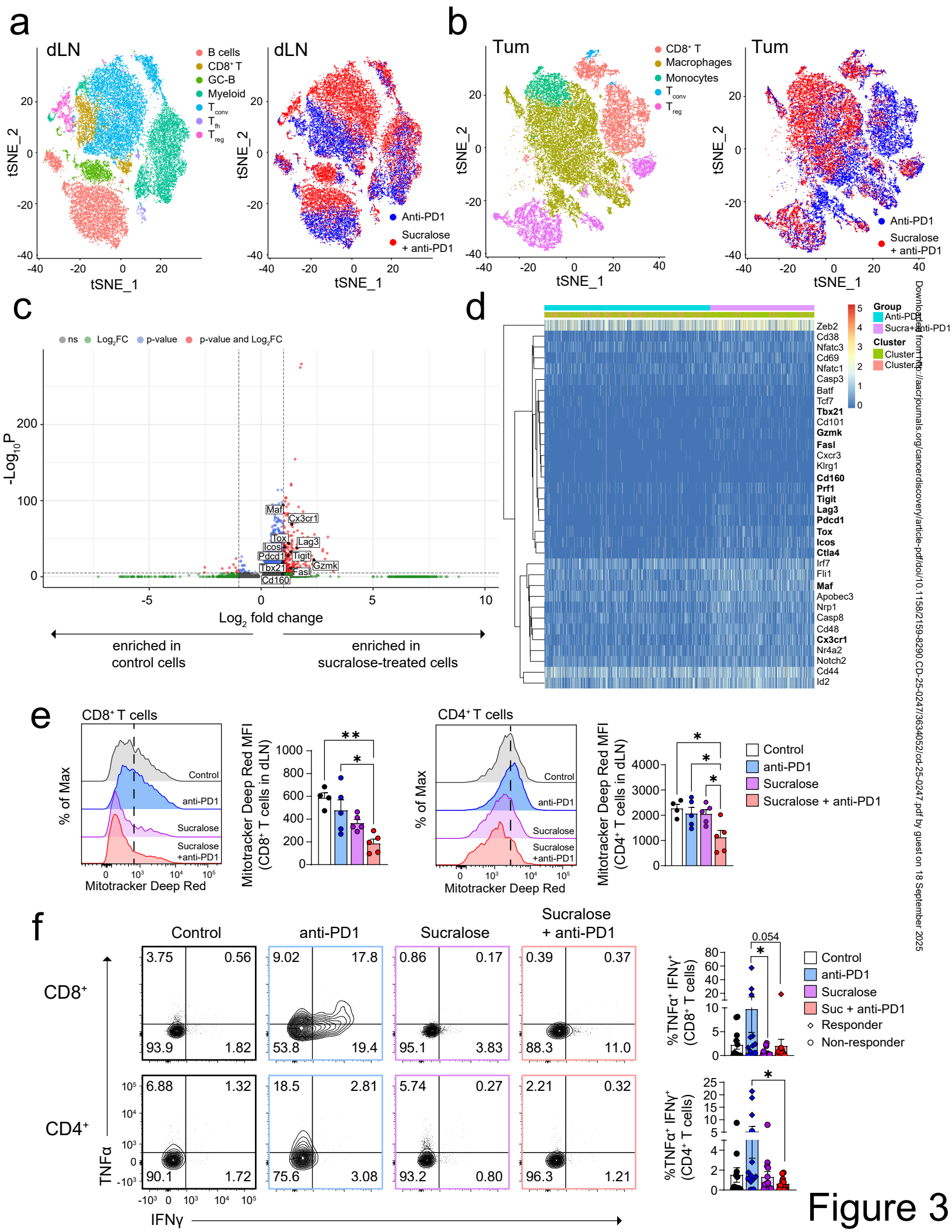

Figure 3

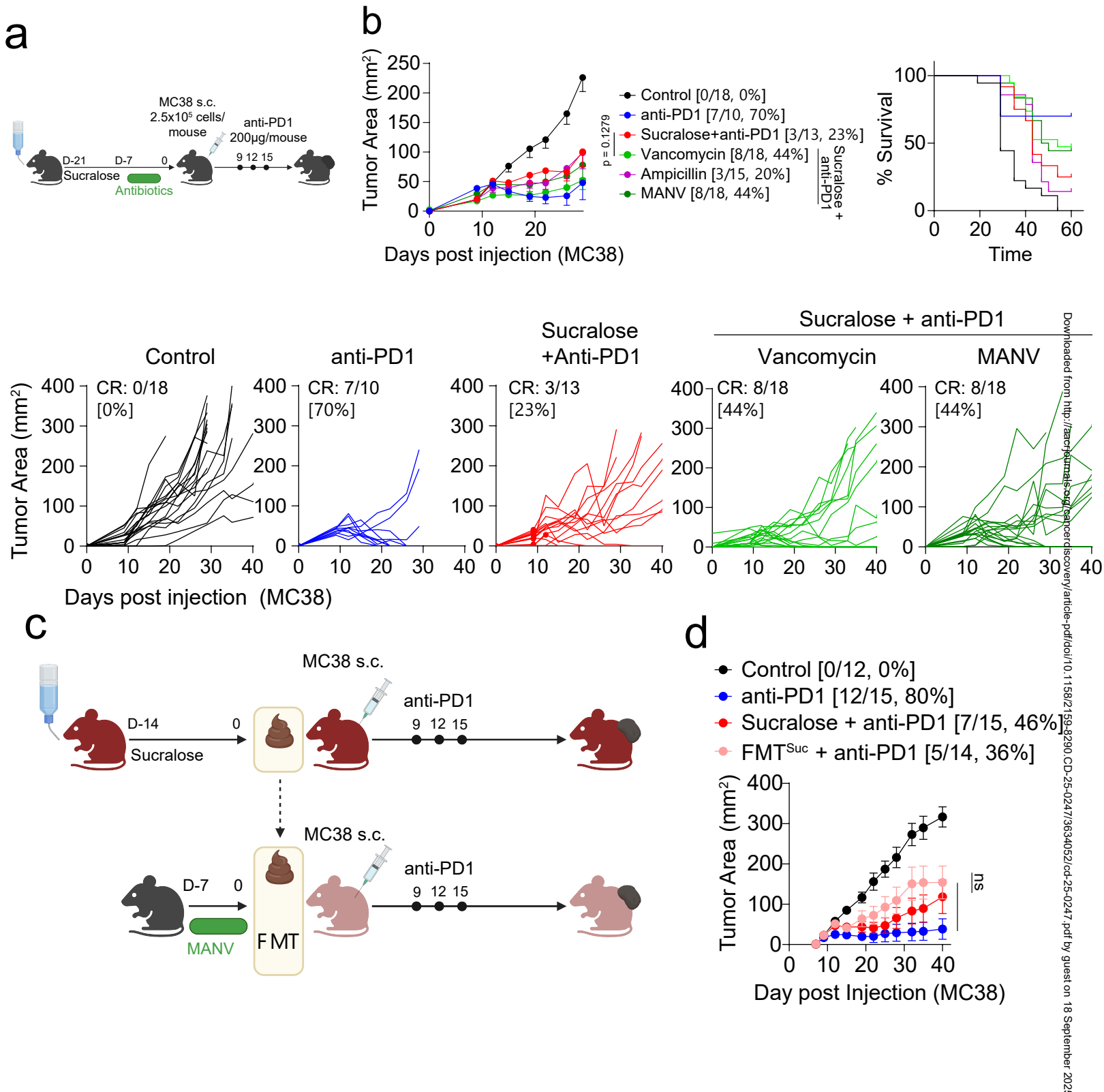

Figure 4

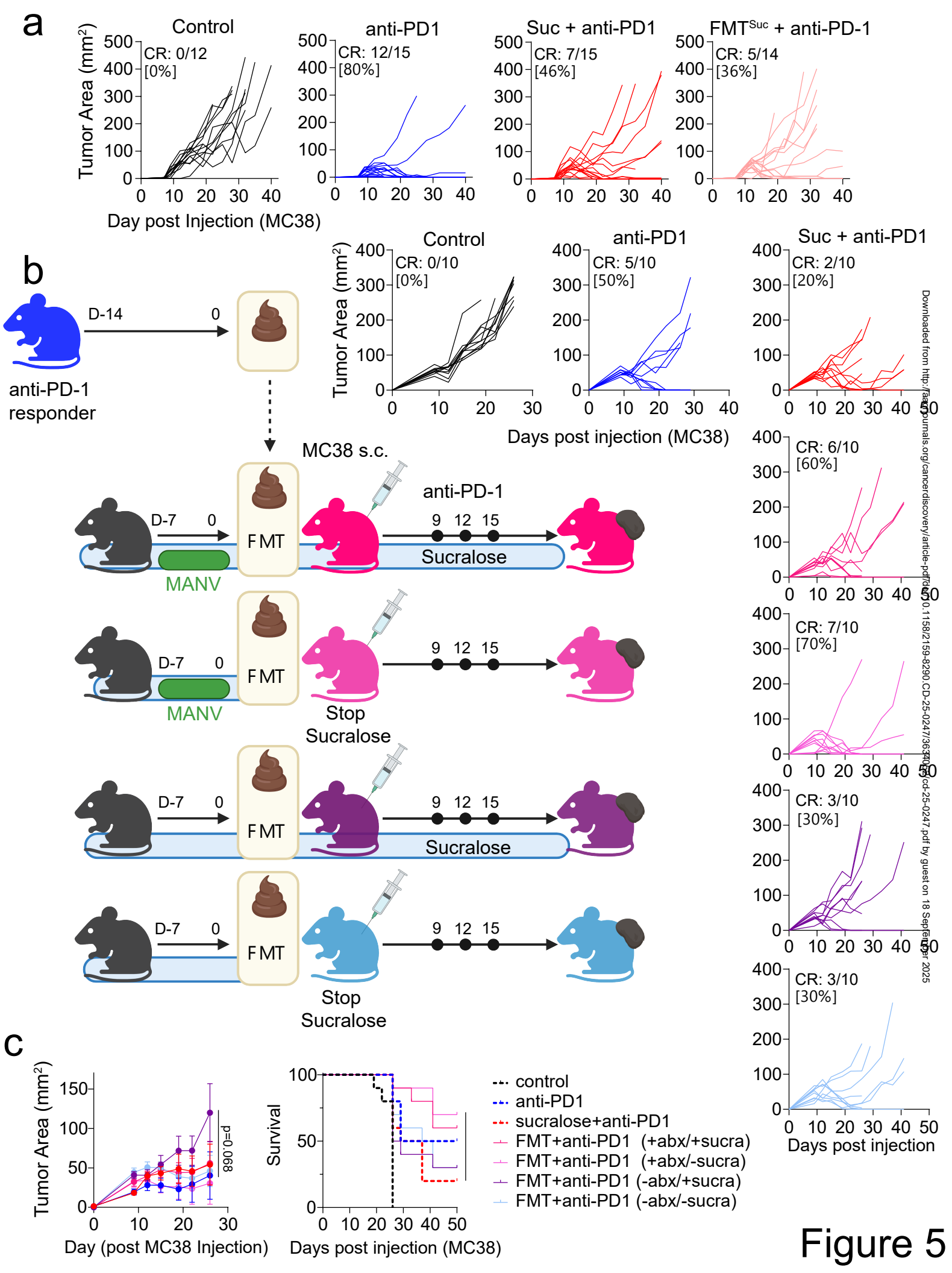

Figure 5

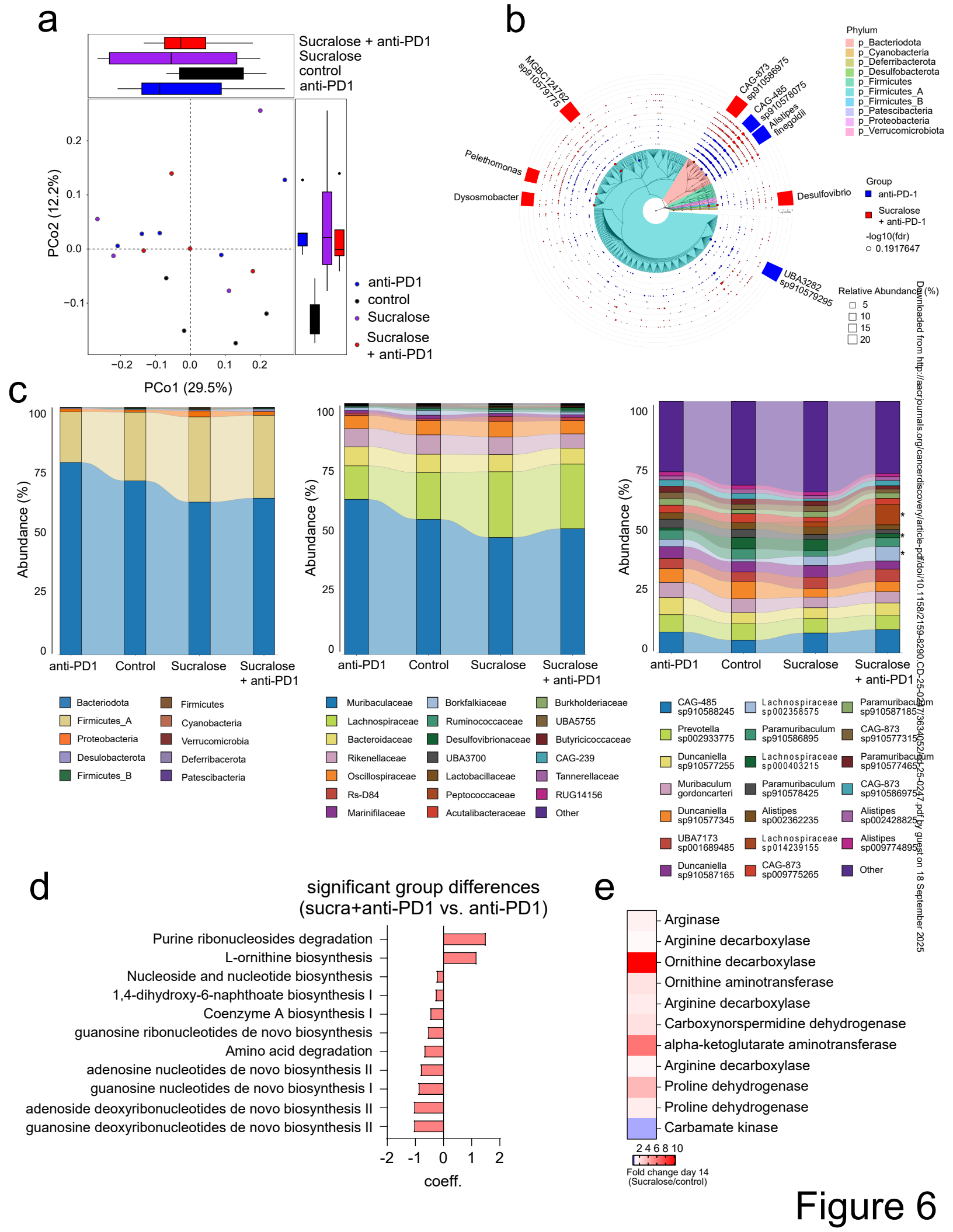

Figure 6

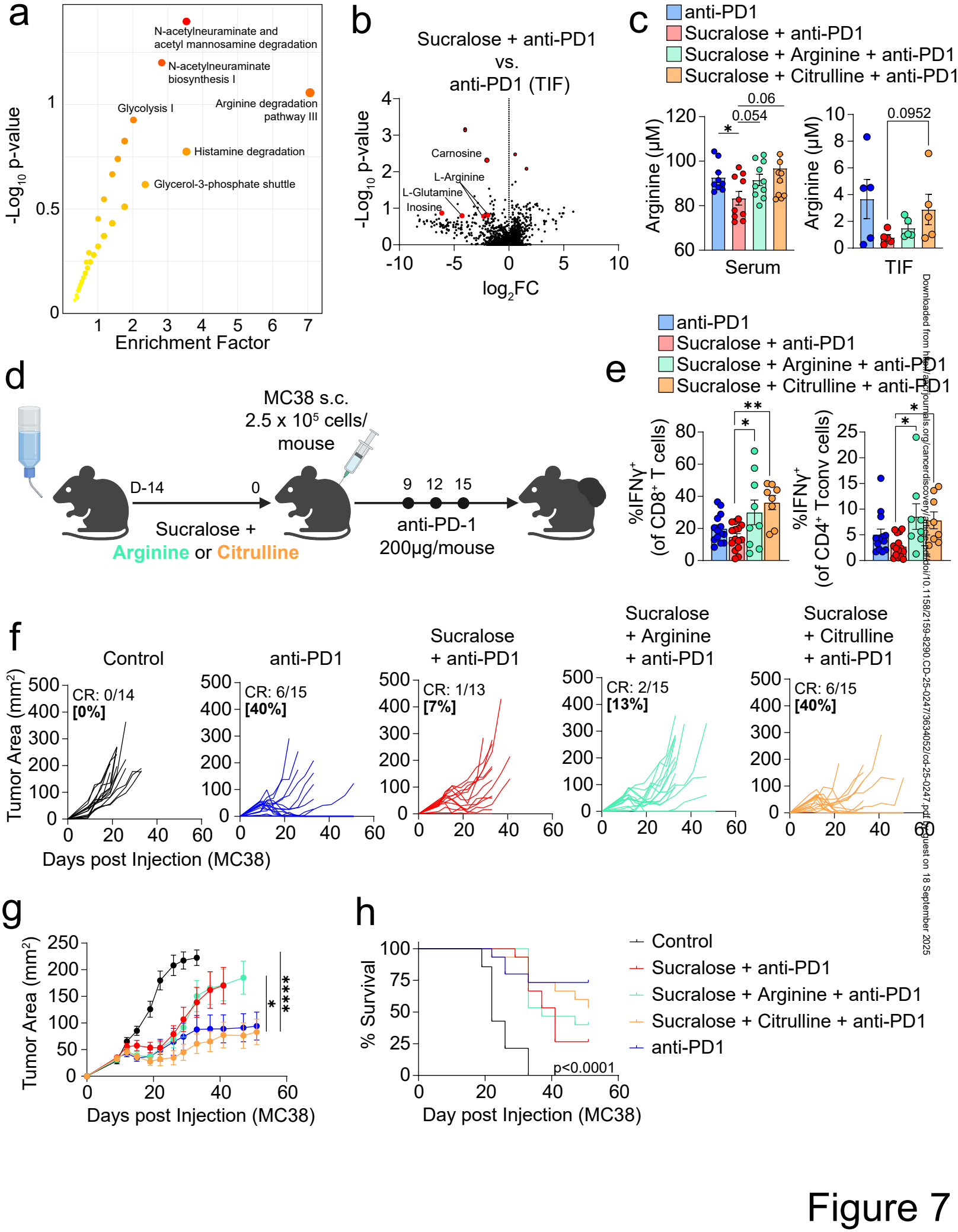

Figure 7